Manuscript prepared for Geosci. Model Dev.
with version 2015/09/17 7.94 Copernicus papers of the LaTeX class copernicus.cls.
Date: 9 June 2017

EcoGEnIE 0.1: Plankton Ecology in a Grid Enabled Integrated Earth systems model

B. A. Ward[1], J. D. Wilson[1], R. Death[1], F. M. Monteiro[1], A. Yool[2], and A. J. Ridgwell[1,3]

[1]School of Geographical Sciences, University of Bristol, Bristol BS8 1SS, UK
[2]National Oceanography Centre, European Way, Southampton SO14 3ZH, UK
[3]Department of Earth Sciences, University of California, Riverside CA, USA

Abstract. We present an extension to the GEnIE Earth System model that explicitly accounts for the growth and interaction of an arbitrary number of plankton species. EcoGEnIE comprises the GOLDSTEIN ocean circulation model, the BIOGEM 'BIOGeochemistry Model', and a new package, called ECOGEM. The new package replaces the implicit parameterisation of plankton-mediated fluxes used in BIOGEM with an explicitly resolved plankton community. Runtime configuration of the model is used to incorporate any number of plankton species, with ecophysiological traits (e.g. growth and grazing rates) assigned according to organism size and functional group (e.g. phytoplankton and zooplankton). We compare results from one configuration of ECOGEM (with eight generic phytoplankton and zooplankton size classes) to climatological and seasonal observations. We also compare the results to a previous iteration of GEnIE with all biological fluxes accounted for by BIOGEM. Global-scale distributions of phosphate, iron, dissolved inorganic carbon, alkalinity and oxygen are similar for both iterations of the model, although a slight deterioration in some fields, relative to the data is observed. The new ecological components of the model show good agreement with both global-scale climatological and local-scale seasonal data. The increased capabilities of the model in this regard will enable future exploration of the ecological community on much longer timescales than have previously been examined in global ocean ecosystem models.

1 Introduction

The marine ecosystem is an integral component of the Earth system. Photosynthetic plankton support almost all life in the ocean, including the vital fisheries providing essential nutrition to more than half the human population (Hollowed et al., 2013). In addition, the oceans sequester massive amounts of carbon away from the atmosphere, playing a key role in moderating the climate. Photosynthetic uptake of carbon in the well-lit ocean surface, followed by the downward transport and deep remineralisation of organic matter result in net increase in the partial pressure of CO_2 at depth, and a net decrease in the ocean surface and atmosphere. This "biological carbon pump" has been estimated to reduce atmospheric carbon concentrations by approximately 200 ppm (Parekh et al.,

2006), and variations in its magnitude have also been cited as possible drivers of glacial-interglacial climate oscillations (Hain et al., 2014).

1.1 Modelling the marine ecosystem

A number of marine biogeochemical models have been developed in an attempt to understand and predict the way the marine carbon cycle functions. The simplest of these ignore the role of biology altogether, treating carbon as an inorganic tracer (Bacastow and Maier-Reimer, 1990). Other, more sophisticated models have attempted to incorporate the biological pump, either in terms of a parameterised flux (e.g. Najjar et al., 1992), or by explicitly including representations of the marine biota (e.g. Wroblewski et al., 1988; Fasham et al., 1990; Anderson and Pondaven, 2003; Aumont et al., 2003).

1.1.1 Biogeochemical fluxes

The biological pump can be incorporated into ocean circulation models without the need to explicitly include state-variables for the biota. Such models of "biogenically induced chemical fluxes" (Maier-Reimer, 1993; Ridgwell et al., 2007) vary in complexity, but can be broadly divided into two categories. Simpler "nutrient-restoring" models quantify the biological uptake of nutrients in terms of the vertical flux required to maintain surface nutrients at observed levels, against the homogenising effects of the ocean circulation (e.g. Bacastow and Maier-Reimer, 1990; Najjar et al., 1992). The vertical flux is then remineralised at depth according to some attenuating profile, such as that of Martin et al. (1987). Within this framework, carbon export is typically calculated from the nutrient flux according to a fixed stoichiometric ratio. Nutrient restoring models typically have between two and four parameters, and in their simplicity they are able to focus on a very specific part of the ecosystem dynamics, namely the downward transport of organic matter. However, because they are based on observations, they are only suitable for diagnostic applications and are unable to model any deviations from the current ocean state.

More sophisticated models of biogenically induced chemical fluxes estimate biological production on the basis of limiting factors, such as temperature, light and the availability of nutrients such as nitrogen, phosphorous and iron. A prescribed fraction of this production is then usually passed to dissolved and particulate forms, with sinking and the subsequent remineralisation of particulate organic matter again accounted for by an attenuating vertical flux. Without the same dependence on observed nutrient distributions, these more advanced models gain a degree of predictive capability that is not available with nutrient restoring models. However, neither type of model is able to represent interactions between any other parts of the ecosystem, simply because they are not resolved.

1.1.2 Resolving ecological guilds

To allow models to respond to changes in ecosystem structure it has been necessary to explicitly resolve the ecosystem itself. Such models have been developed across a wide range of complexities (Kwiatkowski et al., 2014). Among the simplest are 'NPZD' type models, resolving a single nutrient, homogenous phytoplankton and zooplankton communities, and a single detrital pool (Wroblewski et al., 1988; Oschlies, 2001). At the other end of the spectrum, more complex models may include multiple nutrients and several "plankton functional types" (PFTs) (e.g. Aumont et al., 2003; Moore et al., 2002; Le Quéré et al., 2005). What links these models is that the living state variables are very broadly based on ecological guilds (i.e. groups of organisms that exploit similar resources).

While simple models have been shown to be capable of reproducing the bulk properties of ecosystems on both regional and global scales (Palmer and Totterdell, 2001; Spitz et al., 2001; Schartau and Oschlies, 2003; Anderson, 2005) many important biogeochemical processes and climate feedbacks can only be resolved by more complex models (Le Quéré et al., 2005; Hood et al., 2006). Additionally, as the composition of the broad ecological guilds used to define NPZD models will be subject to change through both time and space, PFT models may be more generally applicable because they resolve relatively more fundamental ecological components (Friedrichs et al., 2007). These are the key motivations behind the development of PFT models, in which the broad categories of the NPZD models are replaced with more specific groups based on biogeochemical function. By resolving these key actors in the system, it is possible for the models to capture important climate feedbacks that cannot be represented in simpler models (Le Quéré et al., 2005).

1.1.3 Trait-based models

Alongside their advantages, the current generation of PFT models are faced with two important and conflicting challenges. Firstly, these complex models contain a large number of parameters that are often poorly constrained by observations (Anderson, 2005). Secondly, although PFT models resolve more ecological structure than the preceding generation of ocean ecosystem models, they are rarely general enough to perform well across large environmental gradients (Friedrichs et al., 2006, 2007; Ward et al., 2010). Recent studies have begun to address this problem by focussing on the more general rules that govern diversity (rather than by trying to quantify and parameterise the diversity itself). These 'trait-based' models are beginning to be applied in the field of marine biogeochemical modelling (e.g. Follows et al., 2007; Bruggeman and Kooijman, 2007), with a major advantage being that they are able to resolve greater diversity with fewer specified parameters.

One of the main challenges of this approach is to identify the general rules or trade-offs that govern competition between organisms (Follows et al., 2007; Litchman et al., 2007). These trade-offs are often strongly constrained by organism size. A potentially large number of different plankton size classes can therefore be parameterised according to well known allometric relationships linking

plankton physiological traits to organism size (e.g. Tang, 1995; Hansen et al., 1997). This approach has the associated advantage that the size composition of the plankton community affects the biogeochemical function of the community (e.g. Guidi et al., 2009).

An entirely size-based framework assumes that the fate of organic matter is determined by the size structure of the plankton community. However, taxonomic differences may also require consideration. For example, the high density of taxon specific "ballast" minerals, such as silicate and bicarbonate may increase the sinking rate of particulate organic material (Billet et al., 1983). These 'shell forming' species may also be protected from remineralisation (Armstrong et al., 2002). Physiological and morphological adaptations of marine plankton, such as motile flagella or calcium carbonate appendages may conversely serve to counteract or delay sinking (Smayda, 1970; Padisák et al., 2003).

1.2 A flexible framework for modelling marine ecosystems

Models are indispensable tools in the effort to understand and predict the function of marine ecosystems, but there remain important challenges associated with the complexity of marine ecosystems. While the physical and chemical processes of the solubility pump are reliably described by the Navier-Stokes and carbonate equations, the complex interactions of the food webs underlying the biological pump have (as yet) no such fundamental theoretical framework (Oschlies, 2006). This is because they belong to a extremely heterogeneous and dynamic system, where even the most fundamental biological components are subject to change. A very wide range of marine ecosystem models have been developed, and there are almost as many models as modellers. The wide variety of available mathematical formulations means that model intercomparison can be problematic (Kwiatkowski et al., 2014).

In this paper we present an adaptable modelling framework with an ecological structure that can be easily adapted according to the scientific question at hand. The model is formulated so that all plankton are described by the same set of equations, and any differences are simply a matter of parameterisation. Within this framework, each plankton population is characterised in terms its size-dependent traits and its distinct functional type. The model also includes a realistic physiological component, based on a cell quota model (Caperon, 1968; Droop, 1968) and a dynamic photoacclimation model (Geider et al., 1998). This physiological component, decoupling nutrient uptake and growth, increases model realism, allowing phytoplankton to flexibly take up nutrients according to availability, rather than according to an unrealistically rigid cellular stoichiometry. Such flexible stoichiometry is rarely included in large-scale ocean models, and provides the opportunity to study the links between plankton physiology, ecological competition, and biogeochemistry.

In Section 2 we will briefly outline the Grid Enabled Integrated Earth system model (GEnIE), specifying the ocean circulation and marine biogeochemical modules. In Section 3 we will introduce the new ecological model that has been developed within the GEnIE framework. Section 4 describes

the preliminary model experiments, and Section 5 presents results from the new global model in comparison to observations (where available). Model output is also compared to the pre-existing biogeochemical model (Ridgwell et al., 2007).

2 GEnIE (Grid Enabled Integrated Earth system model)

GENIE is an 'Earth system model of intermediate complexity' (EMIC). GENIE is based on a modularised framework that allows different components of the Earth system, including ocean circulation, ocean biogeochemistry, deep-sea sediments and geochemistry, to be incorporated. The carbon-centric version of GENIE (cGENIE) has been previously applied to explore and understand the interactions between biological productivity, biogeochemistry and climate over a range of timescales and time period (e.g., Ridgwell and Schmidt, 2010; Monteiro et al., 2012; Norris et al., 2013; John et al., 2014; Gibbs et al., 2015; Meyer et al., 2016; Tagliabue et al., 2016). As is common for EMICs, cGENIE features a reduced spatial and temporal resolution in order to facilitate the efficient simulation of the various interacting components. This imposes limits on the resolution of ecosystem dynamics to large-scale annual/seasonal patterns in contrast to higher resolutions often used to model modern ecosystems. However, the motivation for incorporating a new marine ecosystem module into cGENIE is to focus on the explicit interactions between ecosystems, biogeochemistry and climate that are computationally prohibitive in higher resolution models.

2.1 Ocean and Climate Model - C-GOLDSTEIN

The fast climate model, C-GOLDSTEIN features a reduced physics (frictional geostrophic) 3-D ocean circulation model coupled to a 2-D energy-moisture balance model of the atmosphere and a dynamic-thermodynamic sea-ice model. Full descriptions of the model can be found in Edwards and Marsh (2005) and Marsh et al. (2011).

The circulation model calculates the horizontal and vertical transport of heat, salinity, and biogeochemical tracers via the combined parameterisation for isoneutral diffusion and eddy-induced advection (Edwards and Marsh, 2005; Marsh et al., 2011). The degree of spatial and temporal abstraction in C-GOLDSTEIN results in parameter values that are not well known and require calibration against observations. The parameters for C-GOLDSTEIN were calibrated against annual mean climatological observations of temperature, salinity, surface air temperature and humidity using the ensemble Kalman filer (EnKF) methdology (Hargreaves et al., 2004; Ridgwell et al., 2007). The resulting circulation is dynamically similar to that of classical GCMs based on the primitive equations but is significantly faster to run.

2.1.1 Ocean grid resolution

The ocean model is configured on a 36 $\times$ 36 equal-area horizontal grid with 16 logarithmically spaced z-coordinate levels. The horizontal grid is uniform in longitude (10° resolution) and uniform in the sine of latitude (varying in latitude from $\sim$3.2° at the equator to 19.2° near the poles). The thickness of the vertical grid increases with depth, from 80.8 m at the surface, to as much as 765 m at depth. The parameter values for C-GOLDSTEIN used are those reported for the 16-level model in Table S1 of Cao et al. (2009) under "GENIE16". C-GOLDSTEIN is run with 96 time-steps per year. The ocean circulation in this configuration performs well against standard tests of circulation models such as anthropogenic CO_2 and CFC uptake, as well as reproducing the deep ocean radiocarbon (Δ^{14}C) distribution (Cao et al., 2009).

2.2 Biogeochemical model - BIOGEM

The BIOGEM module accounts for the transformation and spatial redistribution of biogeochemical compounds by the marine ecosystem, as well as air-sea gas exchange. A full description can be found in (Ridgwell and Death, in prep.). In place of an explicit representation of living microbial community, the biological (soft-tissue) pump is driven by an implicit (i.e. unresolved) biological community. The biological uptake of carbon and nutrients (such as phosphorus and iron) is limited by light, temperature and nutrient availability. The associated production of organic matter is directly and instantly returned either to dissolved organic matter (DOM), or to inorganic nutrients in the ocean interior according to an attenuating vertical flux (Ridgwell et al., 2007).

- surface inorganic nutrients $\xrightarrow[\text{and export}]{\text{production}}$ DOM and deep inorganic nutrients

Parameters governing biogeochemistry in BIOGEM were previously calibrated against climatological observations of phosphate and alkalinity using an esemble Kalman filter (EnKF) methodology (Ridgwell et al., 2007). Here we use the parameter values for the 16-level model, as reported by Cao et al. (2009). The calculations in BIOGEM are performed once for every 2 time-steps taken by the ocean circulation model (i.e. 48 time-steps per year).

3 Ecological model - ECOGEM

The BIOGEM module does not explicitly resolve the biological community. This simplicity facilitates the efficient modelling of the carbon cycle over long time scales, but the parameterised biological processes are dependent solely on local environmental conditions. In the new ECOGEM module, biological uptake is again limited by light, temperature and nutrient availability, but here it must pass through an explicit and dynamic intermediary plankton biomass pool, before being returned to DOM or dissolved inorganic nutrients.

- surface inorganic nutrients $\xrightarrow{\text{production}}$ plankton biomass $\xrightarrow{\text{export}}$ DOM and deep inorganic nutrients

The explicit plankton community is held entirely within the ECOGEM module, and is not (at present) subject to advection by the physical model. Concentrations of inorganic tracers and details of the physical environment are passed from BIOGEM to ECOGEM, and the ecological community responds by transforming inorganic compounds into living biomass through photosynthesis. The ecological community is also subject to respiration, mortality and internal trophic interactions, and produces both inorganic compounds and organic matter. At the end of each time step, rates of change in inorganic and organic matter attributable to the ecological community are passed back to BIOGEM. This structure is illustrated in Figure 1. (Note that concentrations of non-living organic matter in BIOGEM are not currently made available to ECOGEM, and so the ecological community cannot consume this component of the ecosystem.)

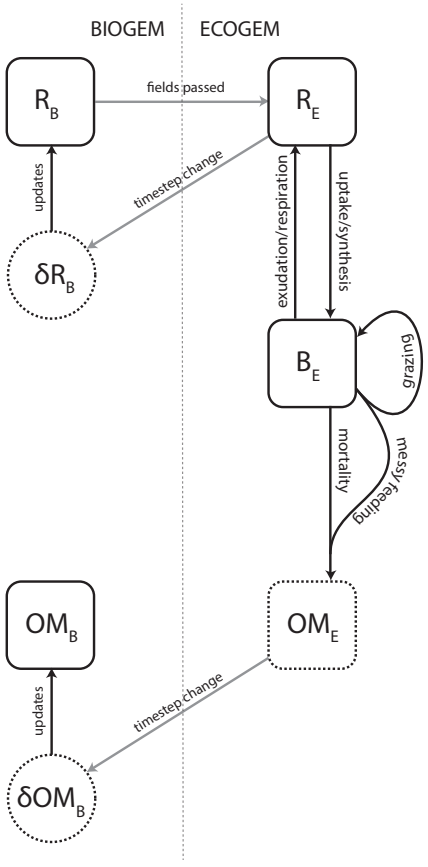

Figure 1. Coupling between BIOGEM and ECOGEM.

In the following section we outline the key state variables directly relating to ecosystem function (Section 3.1), describe the mathematical form of the key rate processes relating to each state variable (Section 3.2) and how they link together (Section 3.3). We will then describe the parameterisation

of the model according to organism size and functional type (Section 3.4). The model equations are modified from those initially presented in Ward et al. (2012).

3.1 State variables

ECOGEM state variables are organised into three matrices (Table 1), representing ecologically-relevant biogeochemical tracers (hereafter referred to as 'nutrient resources'), plankton biomass and organic matter. All these matrices have units of mmol element m^{-3}, with the exception of the dynamic chlorophyll quota, which is expressed in units of mg chlorophyll m^{-3}. The nutrient resource matrix ($\mathbf{R}$) includes I_r distinct inorganic resources. The plankton community ($\mathbf{B}$) is made up of J individual populations, each associated with I_b cellular nutrient quotas. Finally organic matter ($\mathbf{D}$) is made up of K size classes of organic matter, each containing i_d organic nutrient element pools. (Note that strictly speaking organic matter is not explicitly resolved as a state variable, as we currently only resolve the production of organic matter, which is passed to BIOGEM. It is included here for convenience of notation.)

Table 1. State variable index notation.

State variable	Dimensions	Index	Size	Available elements
$\mathbf{R}$	Resource element	i_r	I_r	$DIC, \quad PO_4, \quad Fe$
$\mathbf{B}$	Plankton class	j	J	$1, \quad 2, \quad \ldots, \quad$ J
	Cellular quota	i_b	I_b	$C, \quad P, \quad Fe, \quad Chl$
$\mathbf{D}$	Organic matter size class	k	K	$DOM, \quad POM$
	Detrital nutrient element	i_d	I_d	$C, \quad P, \quad Fe$

3.1.1 Inorganic resources

$\mathbf{R}$ is a vector of length I_r, the number of dissolved inorganic nutrient species.

$$\mathbf{R} = \begin{bmatrix} DIC \\ PO_4 \\ Fe \end{bmatrix} \tag{1}$$

An individual inorganic resource is denoted by the appropriate subscript. For example, PO_4 is denoted R_{PO_4}.

3.1.2 Plankton biomass

$\mathbf{B}$ is a $I_b \times J$ matrix, where I_b is the number of cellular quotas, including chlorophyll, and J is the number of plankton populations.

$$\mathbf{B} = \begin{bmatrix} B_{C,1} & B_{C,2} & \dots & B_{C,J} \\ B_{P,1} & B_{P,2} & \dots & B_{P,J} \\ B_{Fe,1} & B_{Fe,2} & \dots & B_{Fe,J} \\ B_{Chl,1} & B_{Chl,2} & \dots & B_{Chl,J} \end{bmatrix} \quad (2)$$

Each population and element is denoted by an appropriate subscript. For example, the total carbon biomass of plankton population j is denoted $B_{C,j}$, while the chlorophyll biomass of that population is denoted $B_{Chl,j}$. The vector describing the carbon content of all plankton populations is denoted $\mathbf{B}_C$.

This framework can account for competition between (in theory) any number of different plankton populations. The model equations (below) are written in terms of an 'ideal' planktonic form, with the potential to exhibit the full range of ecophysiological traits (among those that are included in the model). Individual populations may take on a realistic subset of these traits, according to their assigned 'plankton functional type' (PFT) (see Section 3.4.1). Each population is also assigned a characteristic size, in terms of equivalent spherical diameter (ESD) or cell volume. Organism size plays a key role in determining each population's ecophysiological traits (see Section 3.4.2).

3.1.3 Organic detritus

$\mathbf{D}$ is a $I_d \times K$ matrix, where I_d is the number of detrital nutrient elements, and K is the number of detrital size classes.

$$\mathbf{D} = \begin{bmatrix} D_{C,1} & D_{C,2} \\ D_{P,1} & D_{P,2} \\ D_{Fe,1} & D_{Fe,2} \end{bmatrix} \quad (3)$$

Each size class and element is denoted by an appropriate subscript. For example, dissolved organic phosphorus (size class $k = 1$) is denoted $D_{1,P}$, while particulate organic iron (size class $k = 2$) is denoted $D_{2,Fe}$.

3.2 Plankton physiology and ecology

The rates of change in each state variable within ECOGEM are defined by a range of ecophysiological processes. These are defined by a set of mathematical functions that are common to all plankton populations. Parameter values are defined in Section 3.4.

3.2.1 Temperature limitation

Temperature affects a wide range of metabolic processes through an Arrenhius-like equation that is here set equal for all plankton.

$$\gamma_{\mathrm{T}} = e^{A(\mathrm{T}-T_{\mathrm{ref}})} \tag{4}$$

The parameter A describes the temperature sensitivity, T is the ambient water temperature in degrees C, and T_{ref} is a reference temperature (also in degrees C) at which $\gamma_{\mathrm{T}} = 1$.

3.2.2 The plankton 'quota'

The physiological status of a plankton population is defined in terms of its cellular nutrient quota, $\mathbf{Q}$, which is the ratio of assimilated nutrient (phosphorus or iron) to carbon biomass. For each plankton population, j, and each planktonic quota, i_b ($\neq C$),

$$Q_{i_b,j} = \frac{B_{i_b,j}}{B_{C,j}} \tag{5}$$

This equation is also used to describe the population chlorophyll content relative to carbon biomass. The size of the quota increases with nutrient uptake, chlorophyll synthesis, or the loss of carbon. The quota decreases through the acquisition of carbon (described below).

Excessive accumulation of P or Fe biomass in relation to carbon is prevented as the uptake or assimilation of each nutrient element is down-regulated as the respective quota becomes full. The generic form of the uptake regulation term for element i_b is given by a linear function of the nutrient status, modified by an additional shape-parameter (h=0.1) that allows greater assimilation under low-to-moderate resource limitation.

$$Q^{\mathrm{stat}}_{i_b,j} = \left(\frac{Q^{\mathrm{max}}_{i_b,j} - Q_{i_b,j}}{Q^{\mathrm{max}}_{i_b,j} - Q^{\mathrm{min}}_{i_b,j}} \right)^h \tag{6}$$

3.2.3 Nutrient uptake

Phosphate and dissolved iron ($i_r = i_b =$ P or Fe) are taken up as functions of environmental availability ($[R_{i_r}]$), maximum uptake rate ($V^{\mathrm{max}}_{i_r,j}$), the nutrient affinity ($\alpha_{i_r,j}$), the quota satiation term, ($Q^{\mathrm{stat}}_{i_b,j}$) and temperature limitation (γ_{T}):

$$V_{i_r,j} = \frac{V^{\mathrm{max}}_{i_r,j} \alpha_{i_r,j} [\mathrm{R_{i_r}}]}{V^{\mathrm{max}}_{i_r,j} + \alpha_{i_r,j} [\mathrm{R_{i_r}}]} Q^{\mathrm{stat}}_{i_b,j} \cdot \gamma_{\mathrm{T}} \tag{7}$$

This equation is effectively equivalent to the Michaelis-Menten type response, but replaces the half-saturation constant with the more mechanistic nutrient affinity, $\alpha_{i_r,j}$.

3.2.4 Photosynthesis

The photosynthesis model is modified from Geider et al. (1998) and Moore et al. (2002). Light-limitation is calculated as a Poisson function of local irradiance (I), modified by the iron-dependent

initial slope of the P-I curve ($\alpha\gamma_{\mathrm{Fe},j}$) and the chlorophyll-*a*-to-carbon ratio ($Q_{\mathrm{Chl},j}$).

$$\gamma_{I,j} = \Big[1 - \exp\Big(\frac{-\alpha \cdot \gamma_{\mathrm{Fe},j} Q_{\mathrm{Chl},j} \cdot I}{P^{\mathrm{sat}}_{\mathrm{C},j}}\Big)\Big] \tag{8}$$

Here $P^{\mathrm{sat}}_{C,j}$ is maximum light-saturated growth rate, modified from an absolute maximum rate of $P^{max}_{C,j}$, according to the current nutrient and temperature limitation terms.

$$P^{sat}_{C,j} = P^{max}_{C,j} \cdot \gamma_T \cdot \min\big[\gamma_{P,j},\, \gamma_{Fe,j}\big] \tag{9}$$

The nutrient-limitation term is given as a minimum function of the internal nutrient status (Droop, 1968; Caperon, 1968; Flynn, 2008), each defined by normalised hyperbolic functions for P and Fe ($i_b =$ P or Fe),

$$\gamma_{i_b,j} = \frac{1 - Q^{\min}_{i_b,j}/Q_{i_b,j}}{1 - Q^{\min}_{i_b,j}/Q^{\max}_{i_b,j}}, \tag{10}$$

The gross photosynthetic rate ($P_{\mathrm{C},j}$) is then modified from $P^{sat}_{C,j}$ by the light-limitation term.

$$P_{\mathrm{C},j} = \gamma_{I,j} P^{\mathrm{sat}}_{\mathrm{C},j} \tag{11}$$

Net carbon uptake, after accounting for the metabolic cost of biosynthesis (ξ), is given by

$$V_{\mathrm{C},j} = P_{\mathrm{C},j} - \xi \cdot 16 V_{\mathrm{P},j} \tag{12}$$

This was originally defined as a loss of carbon as a fraction of nitrogen uptake (Geider et al., 1998). We define it here relative to phosphate uptake, using a fixed N:P ratio of 16.

3.2.5 Photoacclimation

The chlorophyll-to-carbon ratio is regulated as the cell attempts to balance photon capture with the maximum rate at which energy can be used to fix carbon. Depending on this ratio, a certain fraction of newly assimilated nitrogen is diverted to the synthesis of new chlorophyll *a*,

$$\rho_{\mathrm{Chl},j} = \theta^{\max}_{\mathrm{N}} \frac{P_{\mathrm{C},j}}{\alpha \cdot \gamma_{\mathrm{Fe},j} \cdot Q_{\mathrm{Chl},j} \cdot I} \tag{13}$$

where $\rho_{\mathrm{Chl},j}$ is the amount of chlorophyll *a* that is synthesised for every mmol of nitrogen assimilated (mg Chl (mmol N)$^{-1}$). If phosphorus is assimilated at carbon specific rate $V_{\mathrm{P},j}$ (mmol N (mmol C)$^{-1}$ d^{-1}), then the carbon specific rate of chlorophyll *a* synthesis (mg chl (mmol C)$^{-1}$ d^{-1}) is

$$V_{\mathrm{Chl},j} = \rho_{\mathrm{Chl},j} \cdot 16 V_{\mathrm{P},j} \tag{14}$$

3.2.6 Light attenuation

ECOGEM uses a slightly more complex light attenuation scheme than BIOGEM, which simply uses the mean level of photosynthetically available radiation (I) in the surface layer. In ECOGEM, productivity is also restricted to the surface layer, but the light level is calculated as the mean level

of photosynthetically available radiation within the mixed layer, as if the biological population was evenly distributed across the mixed layer (with depth calculated according to Kraus and Turner, 1967) **[NOT SURE IF THIS IS THE RIGHT REF - HAS THIS BEEN USED IN A PUBLISHED VERSION OF GENIE?]**.

If Chl_{tot} is the total chlorophyll concentration in the surface layer, Z_1 is the thickness of the surface grid box and Z_{ML} is the mixed-layer depth, the virtual chlorophyll concentration distributed across the mixed layer is given by

$$Chl_{ML} = Chl_{tot} \frac{Z_1}{Z_{ML}} \tag{15}$$

The combined light-attenuation coefficient attributable to both water and the virtual chlorophyll concentration is given by

$$k_{tot} = k_w + k_{chl} * Chl_{ML} \tag{16}$$

For a given level of photosynthetically available radiation at the ocean surface (I_0), plankton in the surface grid box experience the average irradiance within the mixed layer, which is given by

$$I = \frac{I_0}{k_{tot}} \frac{1}{Z_{ML}} (1 - e^{(-k_{tot} \cdot Z_{ML})}) \tag{17}$$

3.2.7 Predation (including both herbivorous and carnivorous interactions)

Here we define predation simply as the consumption of any living organism, regardless of the trophic level the organism (i.e. phytoplankton, mixotroph, zooplankton, etc.).

The predator-biomass-specific grazing rate of predator (j_{pred}) on prey (j_{prey}) is given by,

$$G_{\mathrm{C},j_{\text{pred}},j_{\text{prey}}} = \gamma_{\mathrm{T}} \cdot \underbrace{\frac{G^{\max}_{\mathrm{C},j_{\text{pred}}} \alpha_{\mathrm{C},j_{\text{pred}}} \mathcal{F}_{\mathrm{C},j_{\text{pred}}}}{G^{\max}_{\mathrm{C},j_{\text{pred}}} + \alpha_{\mathrm{C},j_{\text{pred}}} \mathcal{F}_{\mathrm{C},j_{\text{pred}}}}}_{\text{overall grazing rate}} \cdot \underbrace{\Phi_{j_{\text{pred}},j_{\text{prey}}}}_{\text{switching}} \cdot \underbrace{(1 - e^{\Lambda \cdot \mathcal{F}_{\mathrm{C},j_{\text{pred}}}})}_{\text{prey refuge}} \tag{18}$$

where γ_{T} is the temperature-dependence, $G^{\max}_{\mathrm{C},j_{\text{pred}}}$ is the maximum grazing rate, and $\alpha_{\mathrm{C},j_{\text{pred}}}$ is the grazing 'clearance rate'. The overall grazing rate is a function of total food available to the predator, $\mathcal{F}_{\mathrm{C},j_{\text{pred}}}$. This is given by the product of the prey biomass vector, $\mathbf{B}_{\mathrm{C}}$, and the grazing kernel ($\boldsymbol{\phi}$),

$$\boldsymbol{\mathcal{F}}_{\mathrm{C}} = \boldsymbol{\phi} \mathbf{B}_{\mathrm{C}} \tag{19}$$

The grazing kernel is a $J \times J$ matrix describing the relative availability of each prey population to each predator. Each element is an approximately log-normal function of the predator-to-prey length ratio, $\vartheta_{j_{\text{pred}},j_{\text{prey}}}$, with an optimum ratio of ϑ_{opt} and a geometric standard deviation $\sigma_{j_{\text{pred}}}$.

$$\phi_{j_{\text{pred}},j_{\text{prey}}} = \exp\left[-\left(\ln\left(\frac{\vartheta_{j_{\text{pred}},j_{\text{prey}}}}{\vartheta_{\text{opt}}} \right) \right)^2 / \left(2\sigma^2_{j_{\text{pred}}} \right) \right] \tag{20}$$

We also include an optional 'prey-switching' term, such that predators may preferentially attack those prey that are relatively more available (i.e. active switching, $s = 2$). Alternatively they may

attack prey in direct proportion to their availability (i.e. passive switching, $s = 1$).

$$\Phi_{j_{\mathrm{pred}},j_{\mathrm{prey}}} = \frac{(\phi_{j_{\mathrm{pred}},j_{\mathrm{prey}}} \mathrm{B}_{\mathrm{C},j_{\mathrm{prey}}})^s}{\sum_{j_{\mathrm{prey}}=1}^{J} (\phi_{j_{\mathrm{pred}},j_{\mathrm{prey}}} \mathrm{B}_{\mathrm{C},j_{\mathrm{prey}}})^s} \tag{21}$$

Finally, a prey refuge function is incorporated, such that the overall grazing rate is reduced when the availability of all prey ($\mathcal{F}_{\mathrm{C},j_{\mathrm{pred}}}$) is low. The size of the prey refuge is dictated by the coefficient Λ. The overall grazing response is calculated on the basis of prey carbon. Grazing losses of other prey elements are simply calculated from their stoichiometric ratio to prey carbon, with different elements assimilated according to the predator's nutritional requirements (see below).

$$G_{\mathrm{i_b},j_{\mathrm{pred}},j_{\mathrm{prey}}} = G_{\mathrm{C},j_{\mathrm{pred}},j_{\mathrm{prey}}} \frac{\mathrm{B}_{i_b,j_{\mathrm{prey}}}}{\mathrm{B}_{\mathrm{C},j_{\mathrm{prey}}}} \tag{22}$$

3.2.8 Prey assimilation

Prey biomass is assimilated into predator biomass with an efficiency of $\lambda_{i_b,j_{pred}}$ ($i_b \neq$ Chl). This has a maximum value of $\lambda^{\max}$ that is modified according the quota status of the predator. For elements i_b = P or Fe, prey biomass is assimilated as a function of the respective predator quota. If the quota is full, the element is not assimilated. If the quota is empty, the element is assimilated with maximum efficiency ($\lambda^{\max}$).

$$\lambda_{i_b,j_{\mathrm{pred}}} = \lambda^{\max} Q^{\mathrm{stat}}_{i_b,j} \tag{23}$$

C assimilation is regulated according to the status of the most limiting nutrient element (P or Fe) modified by the same shape-parameter, h, that was applied in Equation 6. If all three quotas are full, C is assimilated at the maximum rate. If any are empty, C assimilation is down-regulated until sufficient quantities of the limiting element(s) are acquired.

$$Q^{\mathrm{lim}}_{i_b,j} = \left(\frac{Q_{i_b,j} - Q^{\mathrm{min}}_{i_b,j}}{Q^{\mathrm{max}}_{i_b,j} - Q^{\mathrm{min}}_{i_b,j}} \right)^h \tag{24}$$

$$\lambda_{C,j_{\mathrm{pred}}} = \lambda^{\max} \min \left(Q^{\mathrm{lim}}_{P,j}, Q^{\mathrm{lim}}_{Fe,j} \right) \tag{25}$$

3.2.9 Respiration

A linear respiration rate is applied to degrade plankton carbon biomass into dissolved inorganic carbon. This is achieved through a J by I_r respiration matrix, $\mathbf{r}$, which is non-zero only for $i_r = DIC$.

3.2.10 Death

All living biomass is subject to a linear mortality rate of m_B. This rate is reduced at very low biomasses (population carbon biomass $\lesssim 1{\times}10{-}6$ mmol C m^{-3}) in order to maintain a viable

population within every surface grid cell ("everything is everywhere, but the environment selects", Baas-Becking, 1934).

$$m_B = m(1 - e^{-10^{10}\mathbf{B}_C}) \tag{26}$$

The low biomass at which a population attains 'immortality' is sufficiently small for that population to have a negligible impact on all other components of the ecosystem.

3.2.11 Sources of detrital matter

Plankton mortality and grazing are the only two sources of organic matter, with partitioning between non-sinking dissolved and sinking particulate phases determined by the parameter β_j.

$$S^{\mathrm{D}}_{i_d,1} = \underbrace{\sum_{j=1}^{J} [\mathrm{B}_{i_d,j}]\beta_j m_{\mathrm{P}}}_{\text{mortality}} + \underbrace{\sum_{j_{\mathrm{pred}}=1}^{J} [\mathrm{B}_{\mathrm{C},j_{\mathrm{pred}}}] \sum_{j_{\mathrm{prey}}=1}^{J} \beta_{j_{\mathrm{prey}}}(1-\lambda_{i_b,j_{\mathrm{pred}}})G_{i_d,j_{\mathrm{pred}},j_{\mathrm{prey}}}}_{\text{messy feeding}} \tag{27}$$

$$S^{\mathrm{D}}_{i_d,2} = \underbrace{\sum_{j=1}^{J} [\mathrm{B}_{i_d,j}](1-\beta_j)m_{\mathrm{P}}}_{\text{mortality}} + \underbrace{\sum_{j_{\mathrm{pred}}=1}^{J} [\mathrm{B}_{\mathrm{C},j_{\mathrm{pred}}}] \sum_{j_{\mathrm{prey}}=1}^{J} (1-\beta_{j_{\mathrm{prey}}})(1-\lambda_{i_b,j_{\mathrm{pred}}})G_{i_d,j_{\mathrm{pred}},j_{\mathrm{prey}}}}_{\text{messy feeding}} \tag{28}$$

A fixed fraction (66%) of the organic matter formed in the surface grid-boxes is partitioned directly into dissolved organic matter. This dissolved organic matter is an explicit tracer that is transported by the ocean circulation model and is degraded back to its constituent nutrients with a fixed turnover time of λ (= 0.5 years).

The remaining fraction (34%) of organic matter is exported vertically from the surface ocean as a flux of particulate organic matter (POM). POM is itself partitioned into two components, a 'labile' component which predominantly remineralises in the upper water column, and a 'refractory' component that is predominantly remineralised in the deep ocean at the seafloor. The net remineralisation at depth z, relative to the export depth z_0 is determined by characteristic length scales (l^{POM} and l^{rPOM} for 'labile' and 'refractory' POM respectively):

$$F^{\mathrm{POM}}_{z} = F^{\mathrm{POM}}_{z=z_0} \cdot \left((1 - r^{\mathrm{POM}}) \cdot \exp(\frac{z_0 - z}{l^{\mathrm{POM}}}) \right) + F^{\mathrm{POM}}_{z=z_0} \cdot \left(r^{\mathrm{POM}} \cdot \exp(\frac{z_0 - z}{l^{\mathrm{rPOM}}}) \right) \tag{29}$$

The remineralisation length scales reflect a constant sinking speed and constant remineralisation rate. All POM reaching the seafloor is remineralised instantaneously.

The production and export of calcium carbonate ($CaCO_3$) by calcifying plankton in the surface ocean is scaled to the export of particulate organic carbon via a spatially-uniform scalar which is modified by a thermodynamically-based relationship with the calcite saturation state. The dissolution of $CaCO_3$ below the surface is treated in a similar way to that of particulate organic matter (equation 29), as described by Ridgwell et al. (2007).

3.2.12 Oxygen

Oxygen production is coupled to photosynthetic carbon fixation via a fixed linear ratio, such that

$$V_{O_2} = -\frac{106}{138}\mathbf{V}_{DIC} \cdot \mathbf{B}_C \tag{30}$$

The negative sign indicates that oxygen is produced as DIC is consumed. Oxygen consumption associated with the remineralisation of organic matter is unchanged relative to BIOGEM.

3.2.13 Alkalinity

Production of alkalinity is coupled to planktonic uptake of PO_4 via a fixed linear ratio, such that

$$V_{Alk} = -16\mathbf{V}_{PO_4} \cdot \mathbf{B}_C \tag{31}$$

The negative sign indicates that alkalinity increases as PO_4 is consumed. Consumption of alkalinity associated with the remineralisation of organic matter is unchanged relative to BIOGEM.

3.3 Differential equations

Differential equations for $\mathbf{R}$, $\mathbf{B}$ and $\mathbf{D}$ are written out in a generalised matrix form, for application to each element in the state variable matrices. The dimensions of each matrix and vector used equations 32 to 34 are given in Table 1. In the following equations the '$\cdot$' symbol denotes a dot product operation, while '$\circ$' denotes entrywise multiplication (the Hadamard product).

Note that while $\mathbf{R}$ and $\mathbf{OM}$ are transported by the physical component of GENIE, living biomass $\mathbf{B}$ is not currently subject to any physical transport. The only communication between biological communities in adjacent grid cells is through the advection and diffusion of inorganic resources and non-living organic matter in BIOGEM. Note that some additional sources and sinks of $\mathbf{R}$, and all sinks of $\mathbf{D}$, are computed in BIOGEM.

3.3.1 Inorganic resources

For each inorganic resource, i_r,

$$\frac{\partial R_{i_r}}{\partial t} = -\underbrace{\mathbf{V}_{i_r} \cdot \mathbf{B}_C}_{\text{uptake}} + \underbrace{\mathbf{r}_{i_r} \cdot \mathbf{B}_C}_{\text{respiration}} \tag{32}$$

3.3.2 Plankton biomass

For each plankton class, j, and internal biomass quota, i_b,

$$\frac{\partial B_{i_b,j}}{\partial t} = +\underbrace{V_{i_b,j}B_{C,j}}_{\text{uptake}} - \underbrace{m_j B_{i_b,j}}_{\text{basal mortality}} + \underbrace{B_{C,j}(\boldsymbol{\lambda}_{i_b} \cdot \mathbf{G}^{\text{gain}}_{i_b})}_{\text{grazing gains}} - \underbrace{r_{i_b,j}B_{C,j}}_{\text{respiration}} - \underbrace{\mathbf{B}_C \cdot \mathbf{G}^{\text{loss}}_{i_b}}_{\text{grazing losses}} \tag{33}$$

3.3.3 Organic detritus

For each detrital nutrient element, i_d, and detritral size class, k

$$\frac{\partial \mathrm{D}_{i_d,k}}{\partial t} = + \underbrace{\Big[\boldsymbol{\beta}_k \circ (1 - \boldsymbol{\lambda}_{i_b})\Big] \mathbf{G}_{i_b} \mathbf{B}_C}_{\text{unassimilated grazing}} + \underbrace{\Big[\boldsymbol{\beta}_k \circ \mathbf{m}\Big] \mathbf{B}_{i_b}}_{\text{other mortality}} \tag{34}$$

The relative fraction of detrital matter passed to DOM is given by the parameter β, which is here assigned a constant value of 0.66 for all populations (Ridgwell et al., 2007).

3.3.4 Coupling to BIOGEM

At the end of each ECOGEM time step, the rates of change in $\mathbf{R}$ and $\mathbf{OM}$ are passed back to BIOGEM. $\partial \mathbf{R}/\partial t$ is used to update DIC, phosphate and iron tracers, while $\partial \mathbf{D}_{DOM}/\partial t$ is added to the dissolved organic matter pools.

The rate of particulate organic matter production, $\partial \mathbf{D}_{POM}/\partial t$ is instantly remineralised at depth using to the standard BIOGEM export functions. $\frac{\partial \mathbf{B}}{\partial t}$ is used only to update the living biomass concentrations within ECOGEM.

3.4 Ecophysiological parameterisation

The model community is made up of a number of different plankton populations, with each one described according to the same set of equations, as outlined above. Differences between the populations are specified according to individual parameterisation of those equations. In the following sections, we describe how the members of the plankton community are specified for evaluation, and how their parameters are assigned according to the organism's size and taxonomic group.

3.4.1 Model structure

The plankton community in ECOGEM is designed to be highly configurable. Each population present in the initial community is specified by a single line in an input text file, which describes the organism size and taxonomic group.

In this configuration we include 16 plankton populations across eight different size classes. These are divided into two PFTs, namely, "Phytoplankton" and "Zooplankton" (see Table 2). The eight phytoplankton populations have nutrient uptake and photosynthesis traits enabled, and predation traits disabled, whereas the opposite is true for the eight zooplankton populations. In future we expect to bring in a wider range of trait-based functional types, including siliceous plankton (e.g. Follows et al., 2007), calcifiers (Monteiro et al., 2016), nitrogen fixers (Monteiro et al., 2010), and mixotrophs (Ward and Follows, 2016).

Table 2. Plankton functional groups and sizes in the standard run.

j	PFT	ESD (μm)	j	Functional Type	ESD (μm)
1	Phytoplankton	0.6	11	Zooplankton	0.6
2	Phytoplankton	1.9	12	Zooplankton	1.9
3	Phytoplankton	6.0	13	Zooplankton	6.0
4	Phytoplankton	19.0	14	Zooplankton	19.0
5	Phytoplankton	60.0	15	Zooplankton	60.0
6	Phytoplankton	190.0	16	Zooplankton	190.0
7	Phytoplankton	600.0	17	Zooplankton	600.0
8	Phytoplankton	1900.0	18	Zooplankton	1900.0

3.4.2 Size-dependent traits

The size-dependent ecophysiological parameters (p) given in Table 3 are assigned as a function of organismal volume ($V = \pi[ESD]^3/6$) according to standard allometric relationships of the form,

$$p = a\Big(\frac{V}{V_0}\Big)^b \tag{35}$$

Here V_0 is a reference value of V_0 = 1 μm^3. The value of p at $V = V_0$ is given by the coefficient a, while the rate of change in p as a function of V is described by the exponent b.

Table 3. Size-dependent ecophysiological parameters (p) and power-law parameters (a and b), such that $p = a\Big(\frac{V}{V_0}\Big)^b$ (Ward and Follows, 2016).

Parameter	Symbol	Power-law parameters		Units
	p	a	b	
Inorganic nutrient uptake				
Maximum uptake rates	$V_{\mathrm{PO_4}}^{\max}$	4.4×10^{-2}	0.06	mmol P (mmol C)$^{-1}$ d^{-1}
	$V_{\mathrm{Fe}}^{\max}$	1.4×10^{-5}	-0.09	mmol Fe (mmol C)$^{-1}$ d^{-1}
Half-saturation concentrations	$k_{\mathrm{PO_4}}$	0.04	0.41	mmol P m^{-3}
	k_{Fe}	8.0×10^{-6}	0.27	mmol Fe m^{-3}
Carbon quotas				
Cell carbon content	Q_{C}	1.45×10^{-11}	0.88	mmol C cell^{-1}
Grazing				
Maximum prey ingestion rate	G_{C}^{max}	21.9	-0.16	d^{-1}

3.4.3 Size-independent traits

A list of size-independent model parameters are listed in Table 4.

Table 4. Size-independent model parameters (Ward and Follows, 2016).

Parameter	Symbol	Value	Units
Nutrient quotas			
Minimum phosphate:carbon quota	$Q_{\mathrm{P}}^{\mathrm{min}}$	2.1×10^{-3}	mmol P (mmol C)$^{-1}$
Maximum phosphate:carbon quota	$Q_{\mathrm{P}}^{\mathrm{max}}$	1.1×10^{-2}	mmol P (mmol C)$^{-1}$
Minimum iron:carbon quota	$Q_{\mathrm{Fe}}^{\mathrm{min}}$	1.0×10^{-6}	mmol Fe (mmol C)$^{-1}$
Maximum iron:carbon quota	$Q_{\mathrm{Fe}}^{\mathrm{max}}$	4.0×10^{-6}	mmol Fe (mmol C)$^{-1}$
Temperature			
Reference temperature	T_{ref}	20	°C
Temperature dependence	A	0.05	-
Photosynthesis			
Maximum Chl-*a*-to-nitrogen ratio	$\theta_{\mathrm{N}}^{\mathrm{max}}$	3.0	mg Chl *a* (mmol N)$^{-1}$
Initial slope of P-I curve	α	3.83×10^{-7}	mmol C (mg Chl *a*)$^{-1}$(μEin m^{-2})$^{-1}$
Cost of biosynthesis	ξ	2.33	mmol C (mmol N)$^{-1}$
Grazing			
Optimum predator:prey length ratio	ϑ_{opt}	10	-
Geometric s.d. of ϑ	σ_{graz}	2.0	-
Total prey half-saturation	$k_{\mathrm{C}}^{\mathrm{prey}}$	5.0	mmol C m^{-3}
Maximum assimilation efficiency	λ^{max}	0.7	-
Grazing refuge parameter	Λ	-1	(mmol C m^{-3})$^{-1}$
Assimilation shape parameter	h	0.1	-
Other loss terms			
Plankton mortality	m	0.05	d^{-1}
Plankton respiration	r_{DIC}	0.05	d^{-1}
Light attenuation			
Light attenuation by water	k_{w}	0.04	m^{-1}
Light attenuation by chlorophyll	k_{Chl}	0.03	m^{-1}(mg Chl)$^{-1}$

3.5 Parameter modifications

As far as possible, the parameter values applied in BIOGEM and ECOGEM were kept as close as possible to previously published versions of the model (Ridgwell et al., 2007; Ward and Follows, 2016). Most of the ecosystem model parameters were taken directly from Ward and Follows (2016), but a few modifications were required to bring ECOGEM into first order agreement with observations and previous iterations of BIOGEM. Firstly, the amount of soluble iron supplied to cGENIE by atmospheric deposition is considerably less than was available in Ward and Follows (2016). With a smaller source of iron, it was necessary to reduce the iron demand of the plankton community, and this was achieved by reducing $Q_{\mathrm{Fe}}^{\mathrm{max}}$ and $Q_{\mathrm{Fe}}^{\mathrm{min}}$ by five-fold ($Q_{\mathrm{Fe}}^{\mathrm{max}}$ from 20 to 4 nmol Fe (mmol C)$^{-1}$, and $Q_{\mathrm{Fe}}^{\mathrm{min}}$ from 5 to 1 nmol Fe (mmol C)$^{-1}$). We also found that the flexible stoichiometry of ECOGEM led to excessive export of carbon from the surface ocean, attributable to higher C:P ratios in organic matter (BIOGEM assumes a Redfieldian C:P of 106). This effect was moderated by

adding the respiration term, which returns a fraction of carbon biomass directly to DIC (it is assumed that other elements are not lost in this way). The additional production of POC also led to increased production of calcium carbonate. This was counteracted by reducing the PIC:POC production ratio from **[X to Y]**.

4 Simulations and Data

4.1 10,000 year spin-up

We ran BIOGEM and ECOGEM each for a period of 10,000 years. These runs were initialised from a homogenous and static ocean, with an imposed constant atmospheric CO_2 concentration of 278 ppm. This configuration is identical to that of Ridgwell and Death (in prep.), with the exception of a few modifications, as described above. Most importantly, the implicit biological production invoked by BIOGEM is replaced with the explicit scheme of ECOGEM, as outlined in the preceding sections.

4.2 Observations

We present model output from the 10,000th year of integration. Although they are not necessarily comparable, we compare results from the pre-industrial configurations of BIOGEM and ECOGEM to contemporary climatologies from a range of sources. Global climatologies of dissolved phosphate and oxygen are drawn from the World Ocean Atlas (WOA 2009), while DIC and alkalinity are taken from Global Ocean Data Analysis Project (GLODAP). Surface chlorophyll concentrations represent a climatological average from 1997 to 2002, estimated by the SeaWiFS satellite. Depth-integrated primary production is from Behrenfeld and Falkowski (1997). All of these interpolated global fields have been re-gridded onto the GEnIE 32x32x16 grid.

Observed dissolved iron concentrations are those published by Tagliabue et al. (2012). These data are too sparse and variable to allow reliable mapping on the GEnIE grid, and are therefore shown as individual data.

Fidelity to the observed seasonal cycle of nutrients and biomass was evaluated against observations from nine Joint Global Ocean Flux Study (JGOFS) sites: the Hawai‘i Ocean Time-series (HOT: 23°N, 158°W), the Bermuda Atlantic Time-series Study (BATS: 32°N, 64°W), the equatorial Pacific (EQPAC: 0°N, 140°W), the Arabian Sea (ARABIAN: 16°N, 62°E), the North Atlantic Bloom Experiment (NABE: 47°N, 19°W), station P (STNP: 50°NS, 145°W), Kerfix (KERFIX: 51°S, 68°E), Antarctic Polar Frontal Zone (APFZ: 62°S, 170°W) and the Ross Sea (ROSS: 75°S, 180°W). Model output for KERFIX and the Ross Sea site was not taken at the true locations of the observations (51°S, 68°E and 75°S, 180°W, respectively). Kerfix was moved to compensate for a poor representation of the Polar Front within the coarse resolution ocean model, while the Ross Sea site does not lie within the GEnIE ocean grid. At each site, the observational data represent the mean

505 daily value within the mixed layer. Data from all years are plotted together as one climatological year.

5 Results

5.1 Biogeochemical variables

We start by describing the global distributions of key biogeochemical tracers that are common to
510 both BIOGEM and ECOGEM.

5.1.1 Global surface values

Annual mean global distributions are presented for the upper 80.8 m of the water column, corresponding to the model surface layer. In Figure 2 we compare output from the two models to observations of dissolved phosphate and iron. Surface phosphate concentrations are broadly similar between
515 the two versions of the model, except that ECOGEM slightly underestimates concentrations in the Southern Ocean. Both versions strongly underestimate surface phosphate in the equatorial and north Pacific, and to a lesser extent in the north and east Atlantic, the Arctic and the Arabian Sea. This is likely attributable in part to the model underestimating the strength of upwelling in these regions. It should also be noted that the observations may in some cases be unrepresentative of the true sur-
520 face layer, when this is significantly less than the model surface layer of 80.8 m. In such cases the observed value will be affected by higher concentrations found above 80.8 m but below the surface mixed layer. Iron distributions are also broadly similar between the two models, with ECOGEM showing slightly lower iron concentrations over most of the ocean.

Figure 3 shows observed and modelled values of inorganic carbon, alkalinity and oxygen. The
525 two models yield very similar surface distributions of the three tracers. DIC and alkalinity are both broadly underestimated relative to observations, while oxygen shows higher fidelity, albeit with artificially high estimates in the equatorial Pacific. This is likely attributable to artificially weak upwelling in this region.

The ocean-to-atmosphere difference in the partial pressure of CO_2 (ΔpCO_2) from the two mod-
530 els is shown in Figure 4. ECOGEM shows weaker CO_2 outgassing in tropical band, with a much stronger ocean-to-atmosphere flux in the Western Arctic.

In Figure 5 we show the annual mean rate of particulate organic matter production in the surface layer. In comparison to BIOGEM, ECOGEM shows elevated POC production in all regions. Production of $CaCO_3$ is globally less variable in ECOGEM than BIOGEM, with notable higher fluxes
535 in the oligotrophic gyres and polar regions.

The relative proportions in which these elements and compounds are exported from the surface ocean are regulated by the stoichiometry of biological production. In BIOGEM, carbon and phosphorus production are rigidly coupled through a fixed ratio of 106:1, while POFe:POC and $CaCO_3$:POC

production ratios are regulated as a function of environmental conditions. In ECOGEM, phosphorus,
540 iron and carbon production are all decoupled through the flexible quota physiology, which depends on both environmental conditions, and the status of the food-web. Only $CaCO_3$:POC production ratios are regulated via the same mechanism in the two models (although we reduced the average $CaCO_3$:POC ratio in BIOGEM to compensate for the elevated POC production relative to POP).

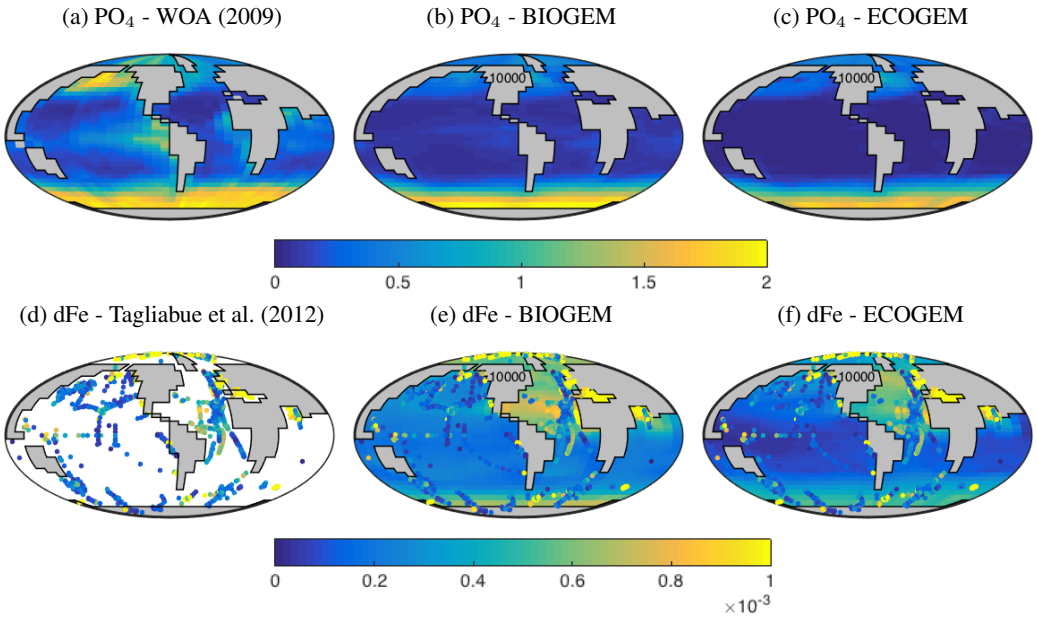

Figure 2. Surface concentrations of dissolved inorganic nutrients.

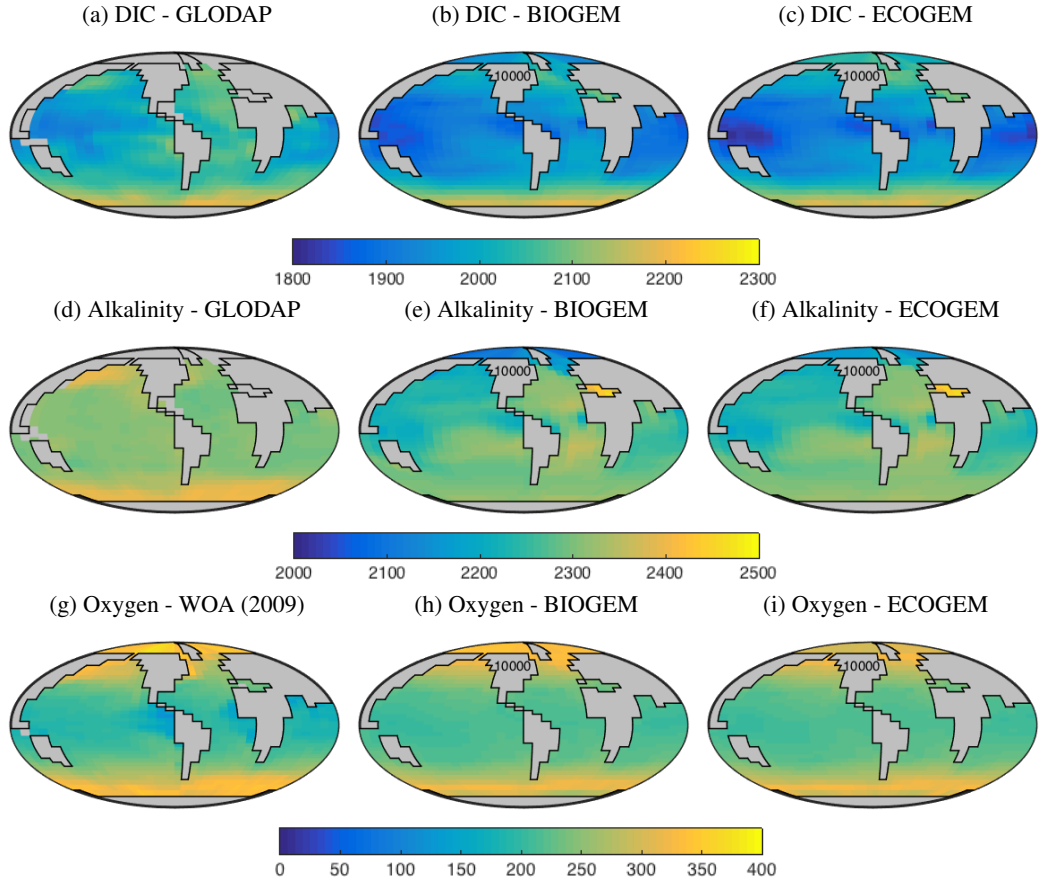

Figure 3. Surface concentrations of dissolved inorganic carbon, alkalinity and dissolved oxygen.

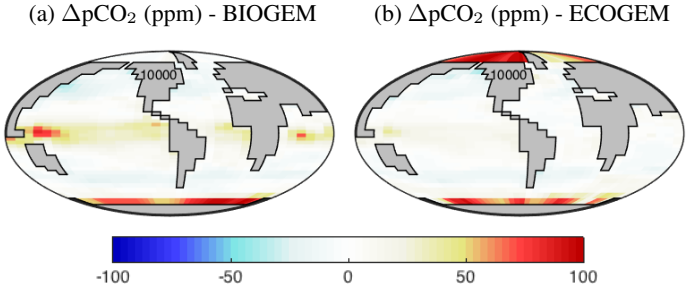

Figure 4. (Preindustrial) surface ΔpCO_2.

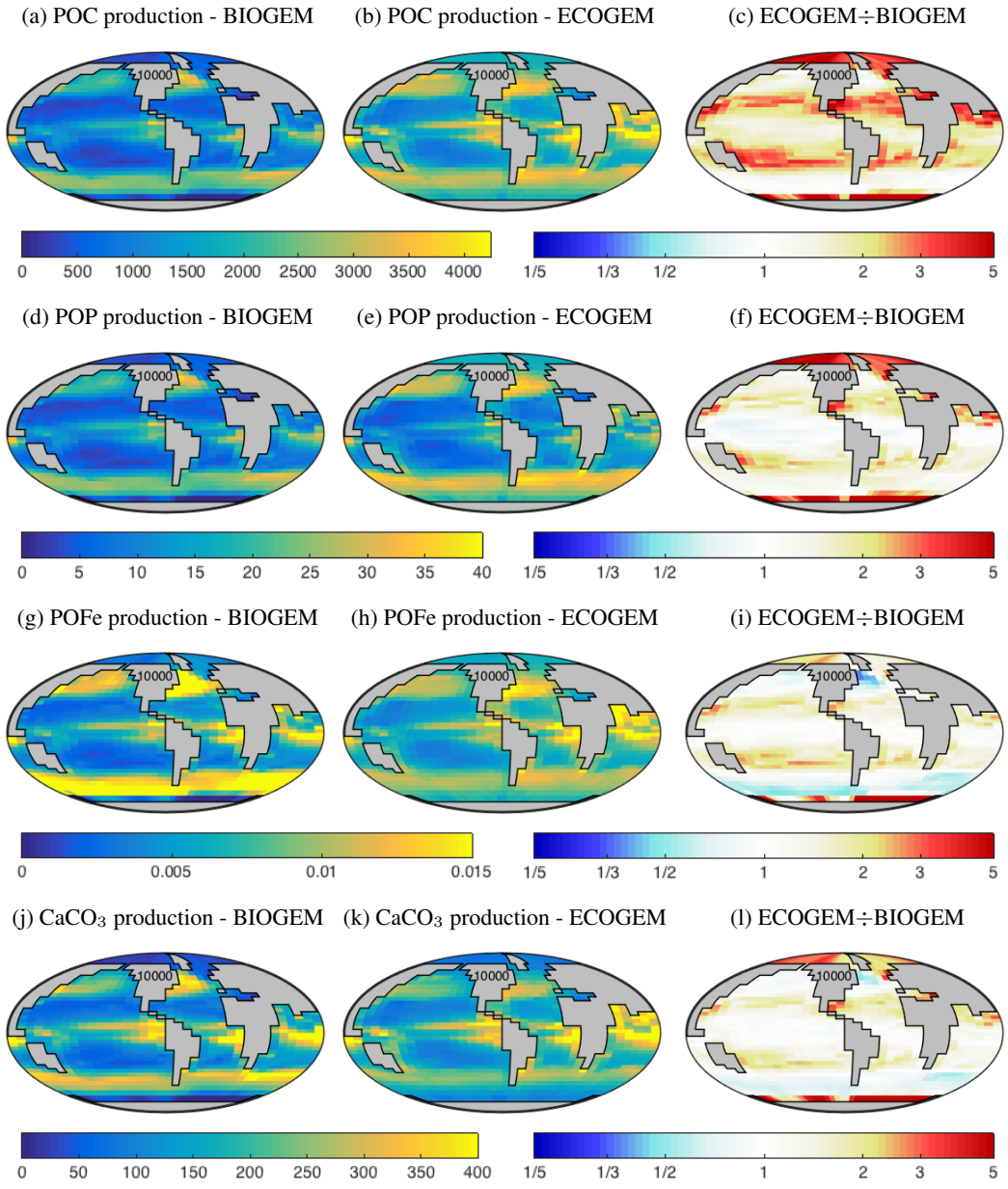

Figure 5. Particulate matter production (and export from the surface layer). The right-hand column indicates the relative increase or decrease in ECOGEM, relative to BIOGEM.

5.1.2 Basin-averaged depth profiles

In this section we present meridional depth distribution of key biogeochemical tracers, averaged across each of the three main ocean basins, as shown in Figure 6. Figure 7 shows that the vertical distribution of dissolved phosphate is very similar between the two models, with ECOGEM showing a slightly stronger sub-surface accumulation in the northern Indian Ocean.

The vertical distributions shown in Figure 8 reveal that dissolved iron is lower throughout the ocean in ECOGEM, relative to BIOGEM, particularly below 1500 m. Differences are less obvious at intermediate depths. (Observations are currently too sparse to estimate reliable basin-scale distributions of dissolved iron; see Tagliabue 2016.)

Figure 9 shows that while BIOGEM reproduces observed DIC distributions very well, ECOGEM overestimates concentrations within the Indian and Pacific Oceans. The total oceanic DIC inventory increased by just under 2% from 0.299 mol C in BIOGEM to 0.304 in ECOGEM (with a fixed atmospheric CO2 concentration of 278 ppm). Otherwise the two models show broadly similar distributions, with the most pronounced differences (as for PO_4) in the northern Indian Ocean.

Alkalinity shows some pronounced differences between the two models, particularly in the Indian Ocean. In this region ECOGEM shows excessive accumulation of alkalinity at $\sim$1000 m depth (this also occurs to a lesser degree in the north Pacific). The reason for this accumulation is not clear, but it is not seen in BIOGEM. It may be possible to overcome this issue if ECOGEM can be subjected to the same degree of parameter tuning as BIOGEM.

BIOGEM correctly captures the invasion of O_2 into the ocean interior through the Southern Ocean and North Atlantic. These patterns are also seen in ECOGEM, although concentrations in the deep ocean are too low, especially in the Indian and Pacific Oceans. This is presumably as a consequence of greater export and remineralisation of organic carbon in ECOGEM leading to more oxygen consumption. The region of elevated PO_4, DIC and alkalinity in the Indian Ocean is also associated with a large anoxic region. Anoxia is also too prevalent in the Pacific.

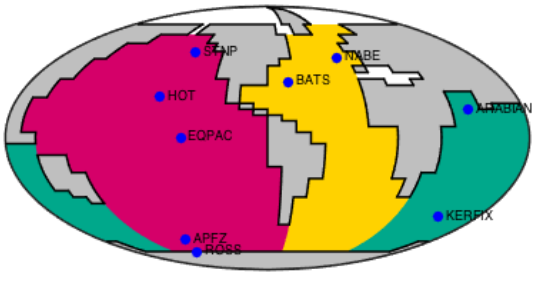

Figure 6. Spatial definition of the three ocean basins used in Figures 7 to 11. Locations of the JGOFS time-series sites are indicated with blue dots.

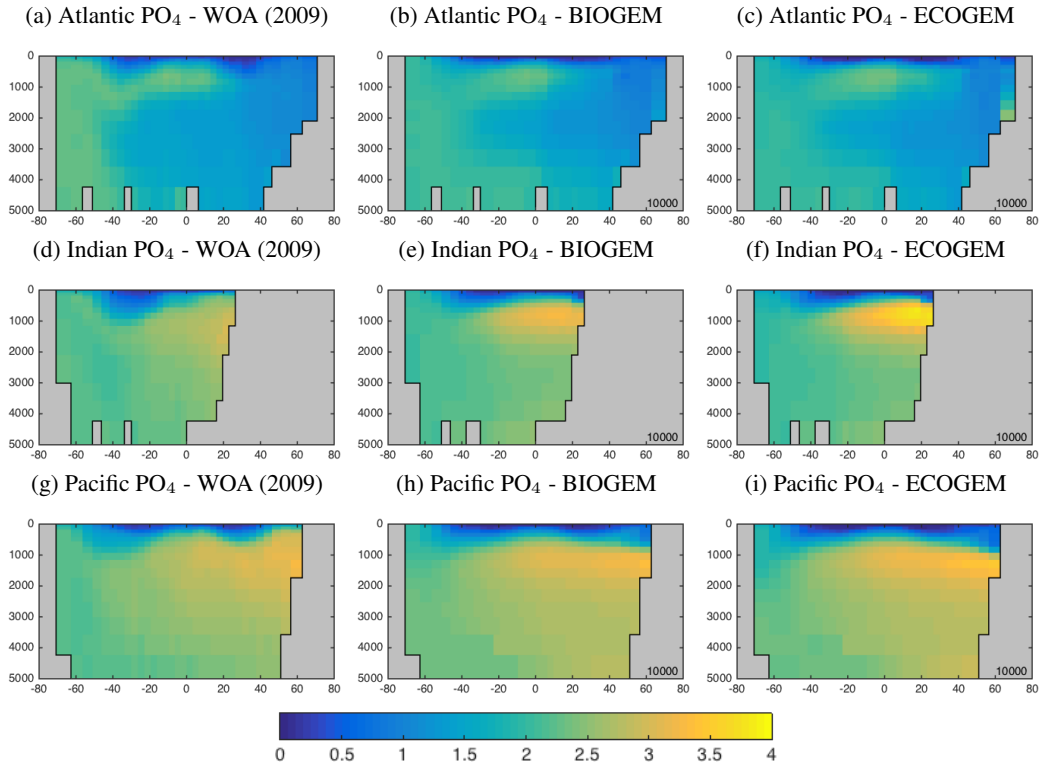

Figure 7. Basin-averaged meridional-depth distribution of phosphate.

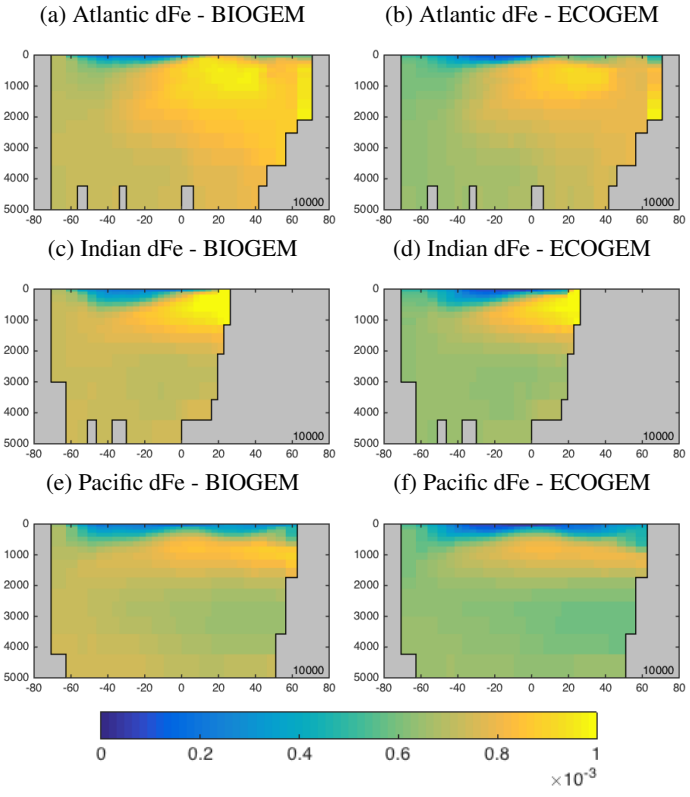

Figure 8. Basin-averaged meridional-depth distribution of total dissolved iron (dFe).

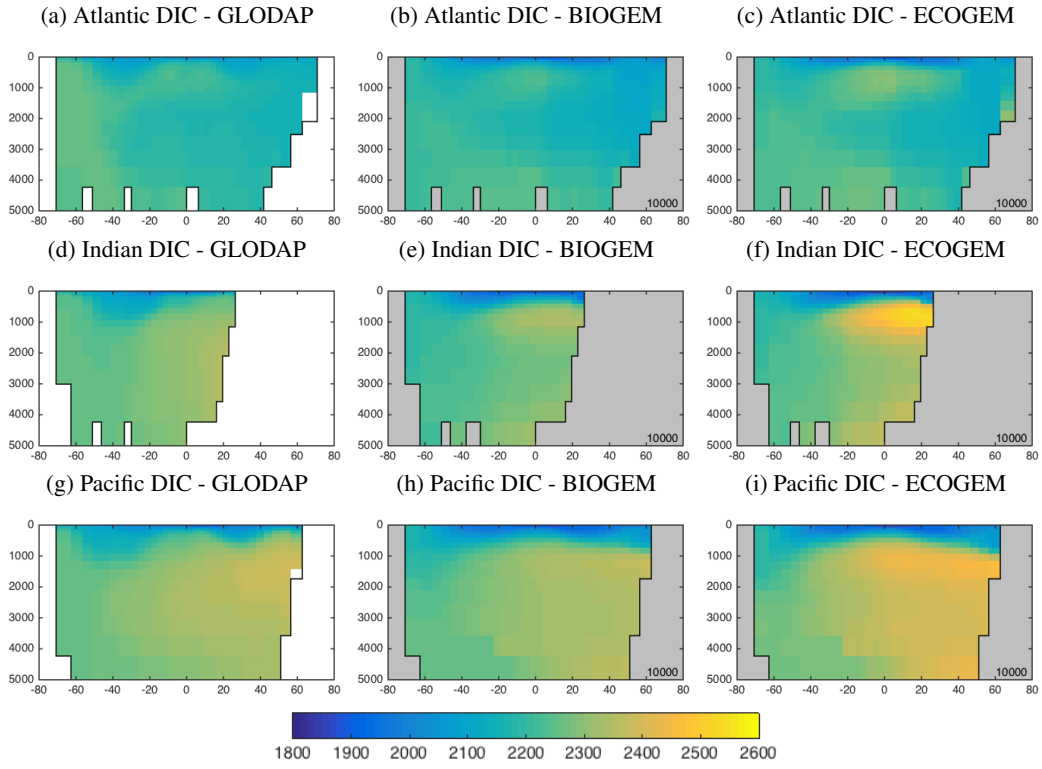

Figure 9. Basin-averaged meridional-depth distribution of DIC.

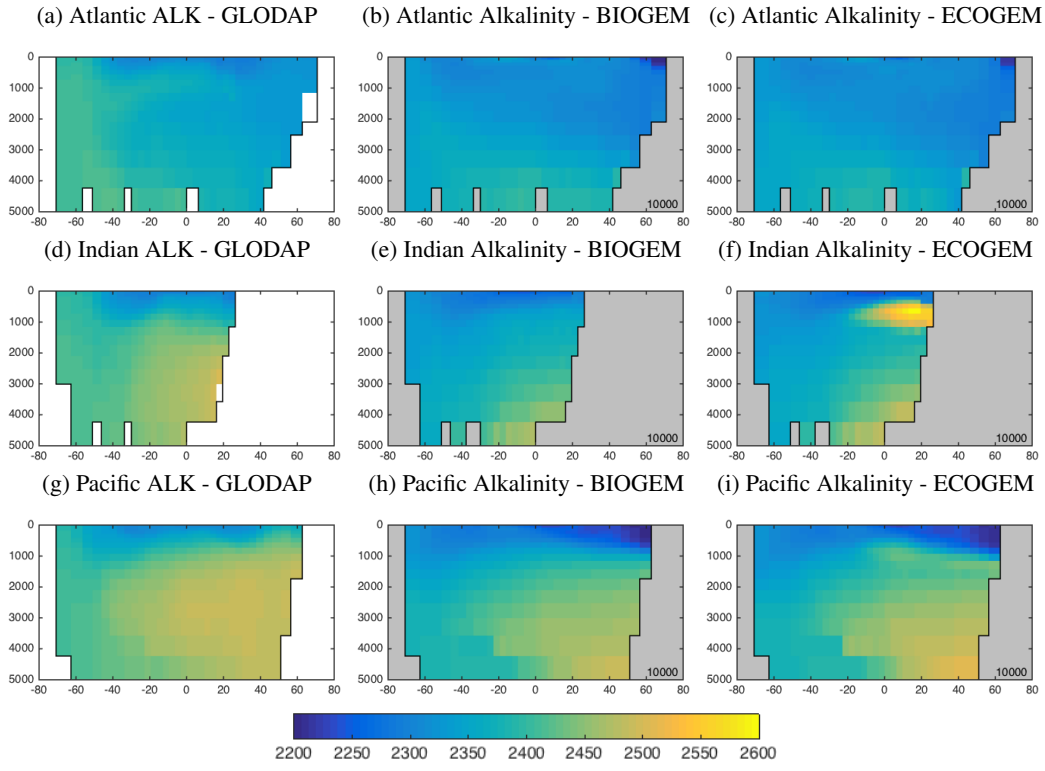

Figure 10. Basin-averaged meridional-depth distribution of alkalinity.

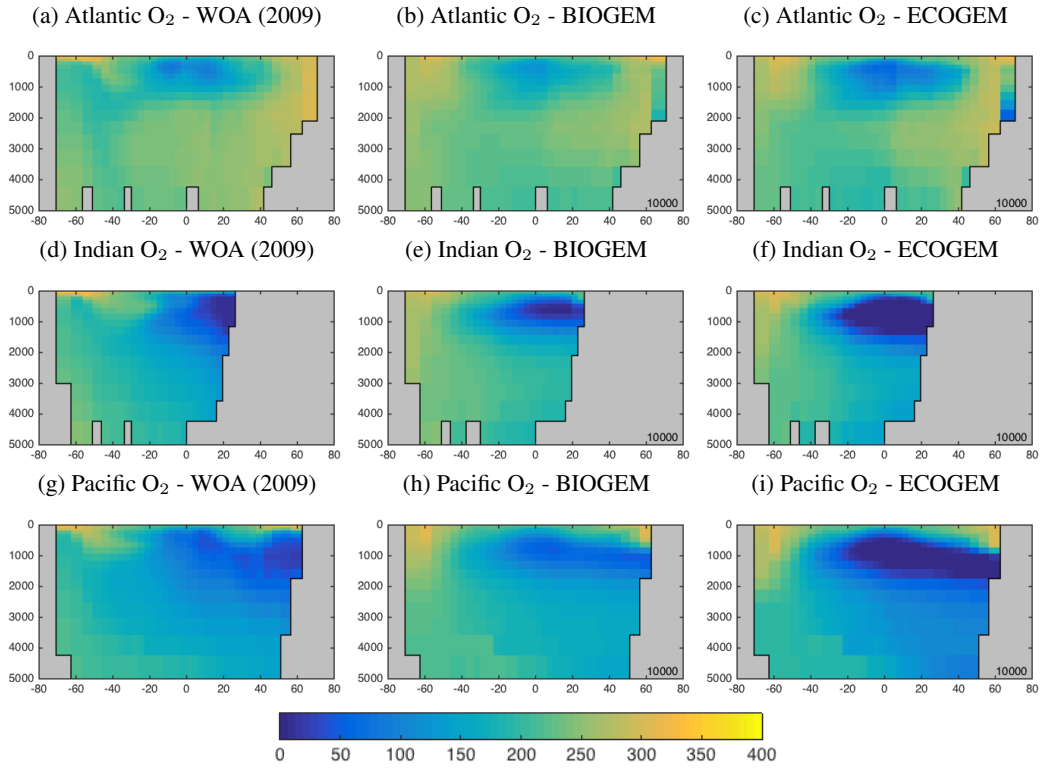

Figure 11. Basin-averaged meridional-depth distribution of phosphate.

5.1.3 Time-series

570 Figures 12 and 13 we compare the seasonal cycles of surface nutrients (phosphate and iron) at nine Joint Global Ocean Flux Study (JGOFS) sites. ECOGEM mostly shows lower PO_4 and Fe concentrations at the ocean surface, with greater seasonal variability.

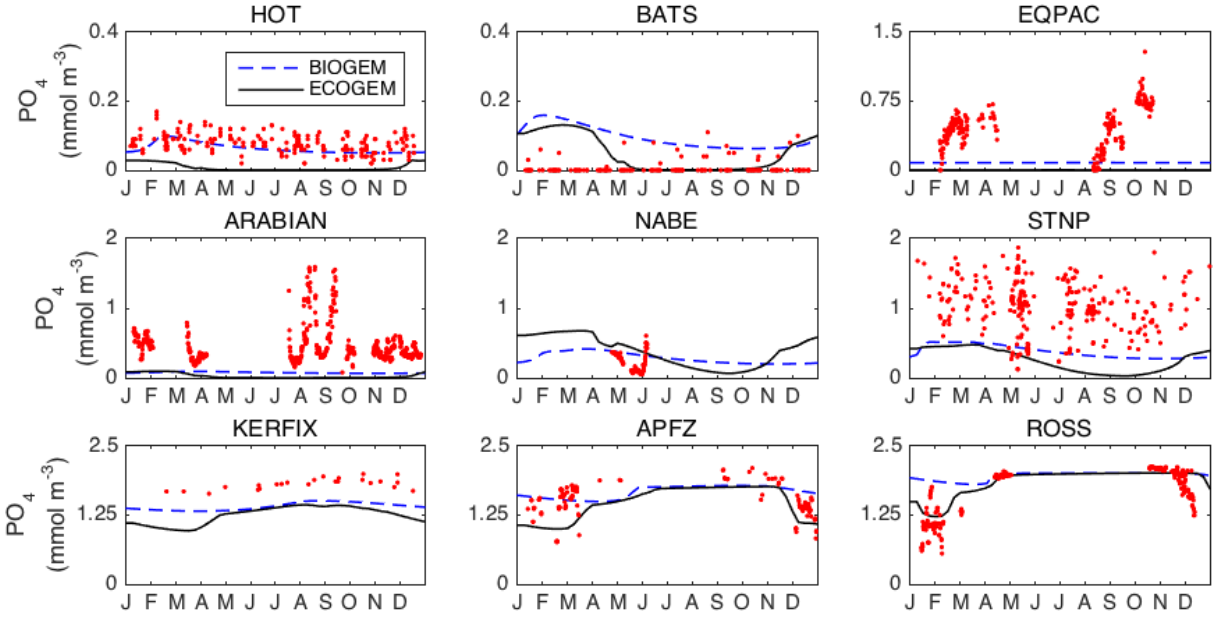

Figure 12. Annual cycle of surface PO_4 at 9 time-series sites in BIOGEM and ECOGEM. Red dots indicate climatological observations, while the lines represent modelled surface PO_4concentrations. Locations of the time-series are indicated in Figure 6.

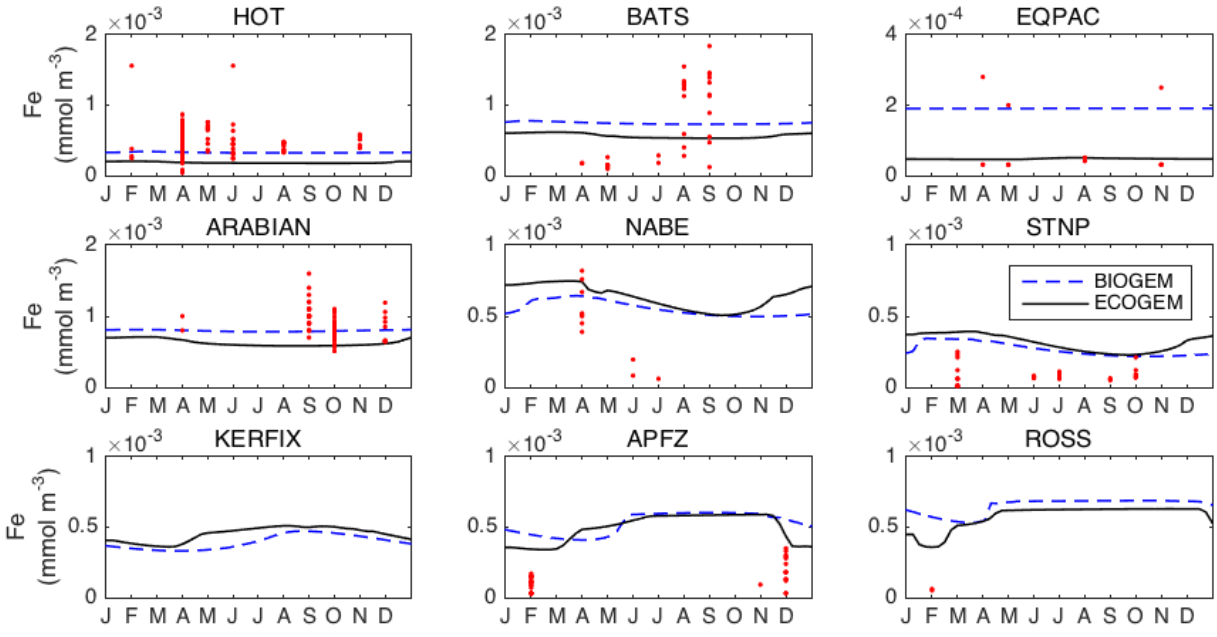

Figure 13. Annual cycle of surface dissolved iron at 9 time-series sites in BIOGEM and ECOGEM. Red dots indicate climatological observations, while the lines represent modelled surface iron concentrations. Locations of the time-series are indicated in Figure 6.

5.2 Ecological variables

Moving on from the core components that are common to both models, we present a range of ecological variables that are exclusive to ECOGEM. As before, we begin by presenting the annual mean global distributions in the ocean surface layer, comparing total chlorophyll and primary production to satellite-derived estimates (Figure 14). We then look in more detail at the community composition, with Figure 15 showing the carbon biomass within each plankton population. Figure 16 then shows the degree of nutrient limitation within each phytoplankton population. Finally, in Figure 18, we show the seasonal cycle of community and population level chlorophyll at each of the nine JGOFS time-series sites.

5.2.1 Global surface values

Figure 14 reveals that ECOGEM shows some limited agreement with the satellite-derived estimate of global chlorophyll. As expected, chlorophyll biomass is elevated in the high-latitude oceans relative to lower latitudes. The sub-tropical gyres show low biomass, but the distinction with higher latitudes is not as clear as in the satellite estimate. The model also shows a clear lack of chlorophyll in equatorial and coastal upwelling regions, relative to the satellite estimate. The model predicts higher chlorophyll concentrations in the Southern Ocean, although this may, in part, be related to the satellite algorithm overestimating concentrations in these regions (Dierssen, 2010).

Modelled primary production correctly increases from the oligotrophic gyres towards high latitudes and upwelling regions, but variability is much lower than in the satellite estimate. Specifically, the model and satellite estimates yield broadly similar estimates in the oligotrophic gyres, but the model does not attain the high values seen at higher latitudes and in coastal areas. This latter mismatch is most likely due to the low spatial resolution of GEnIE.

Figure 15 shows the modelled carbon biomass concentrations in the surface layer, for each modelled plankton population. The smallest (0.6 μm) phytoplankton size class is evenly distributed in the low-latitude oceans between 40° N and S, but is largely absent nearer to the poles. The 1.9 μm phytoplankton size class is similarly ubiquitous at low latitudes, albeit with somewhat higher biomass, and its range extends much further towards the poles. With increasing size, the larger phytoplankton are increasingly restricted to highly productive areas, such as the sub-polar gyres and upwelling zones.

Perhaps as expected, zooplankton size classes tend to mirror the biogeography of their phytoplankton prey. The smallest (1.9 μm) size class is found primarily at low latitudes, although a highly variable population is found at higher latitudes. This population is presumably supported by grazing on the larger 6 μm size class (with very low efficiency dictated by the unfavourable predator-prey length ratio). Larger zooplankton size classes follow a similar pattern to the phytoplankton, moving

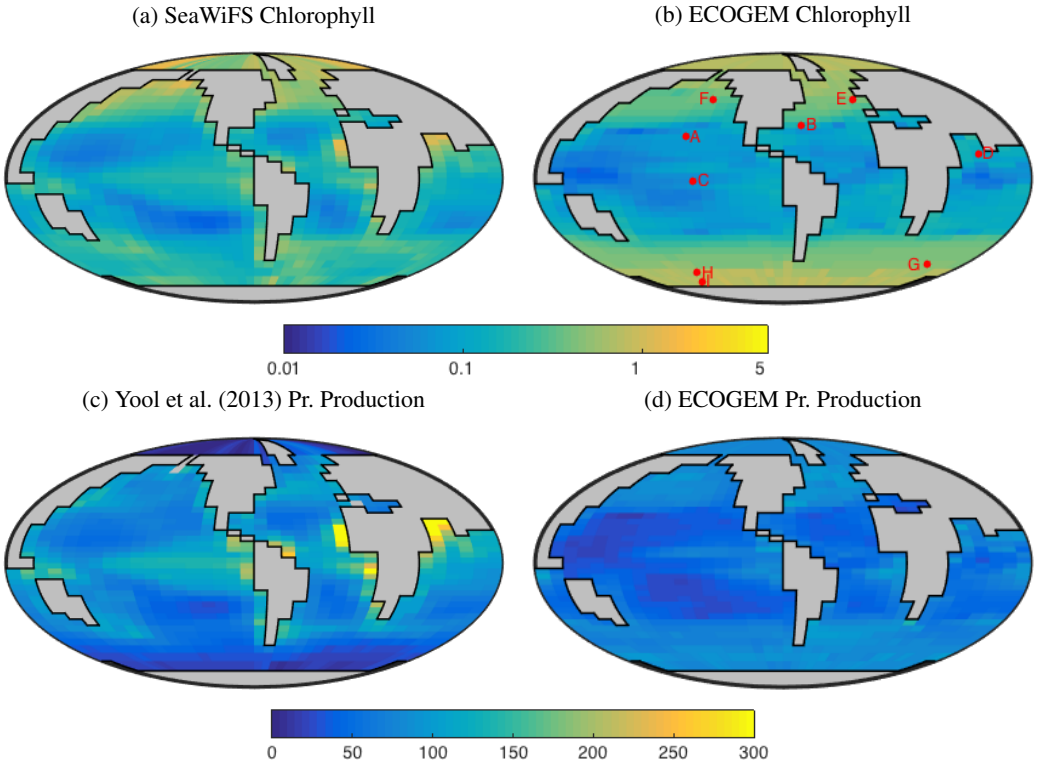

Figure 14. Satellite-derived (left) and modelled (right) surface chlorophyll *a* concentration and depth-integrated primary production. The satellite-derived estimate of primary production is a composite of three products (Behrenfeld and Falkowski, 1997; Carr et al., 2006; Westberry et al., 2008), as in Yool et al. (2013, Figure 12).

from a cosmopolitan but homogenous distribution in the smaller size classes, towards spatially more variable distributions among the larger organisms.

The degree of nutrient limitation within each phytoplankton size class is shown in Figure 16. The two-dimensional colour-scale indicates decreasing iron limitation from left to right, and decreasing phosphorus limitation from bottom to top. White is therefore nutrient replete, blue is phosphorus limited, red is iron limited, and magenta is phosphorus-iron co-limited. The figure demonstrates that the smallest size class is not nutrient limited in any region. The increasing saturation of the colour scale in larger size classes indicates an increasing degree of nutrient limitation. As expected, nutrient limitation is strongest in the highly stratified low latitudes. A stronger vertical supply of nutrients at higher latitudes is associated with weaker nutrient limitation, although nutrient limitation is still significant among the larger size classes. Consistent with observations (Moore et al., 2013), phosphorus limitation is restricted is restricted to low latitudes. Iron limitation dominates in high latitude regions. Among the larger size classes the upwelling zones appear to be characterised by iron-phosphorus co-limitation.

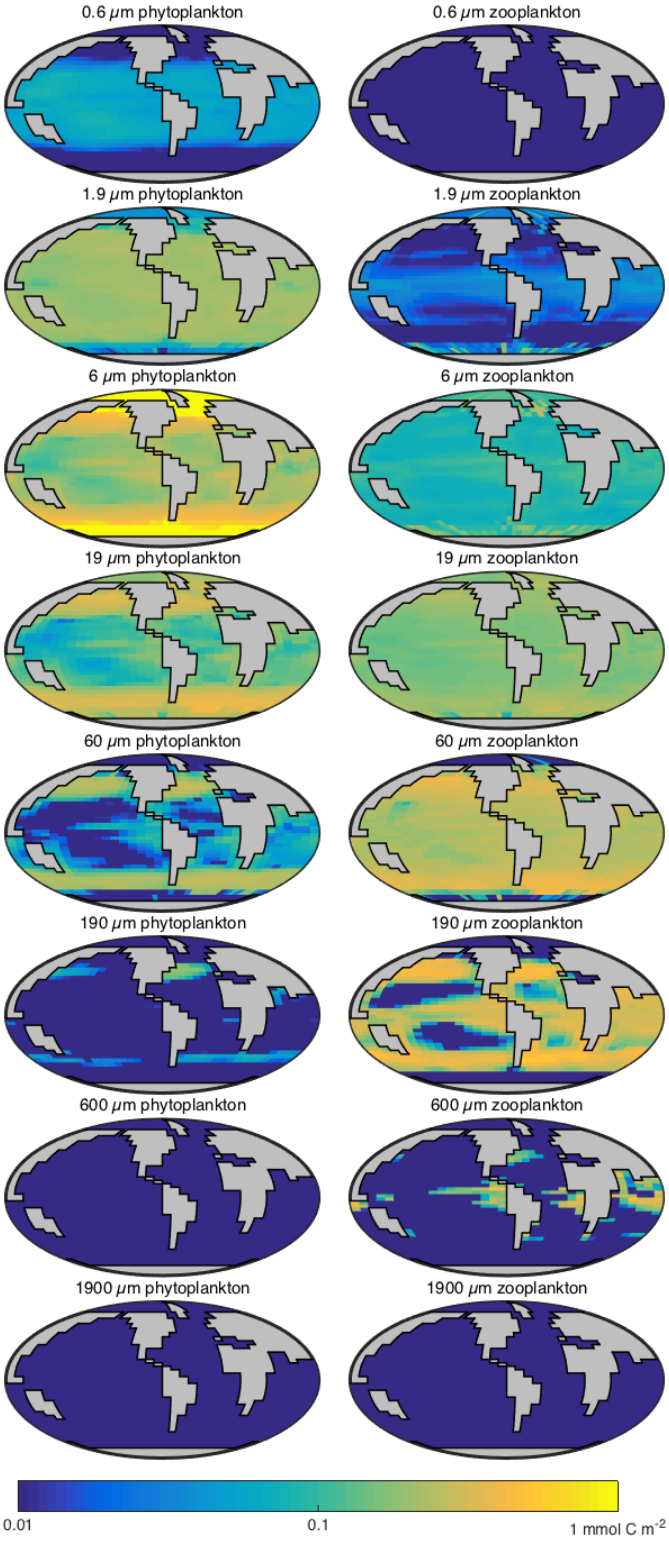

Figure 15. Surface concentrations of carbon biomass in each population.

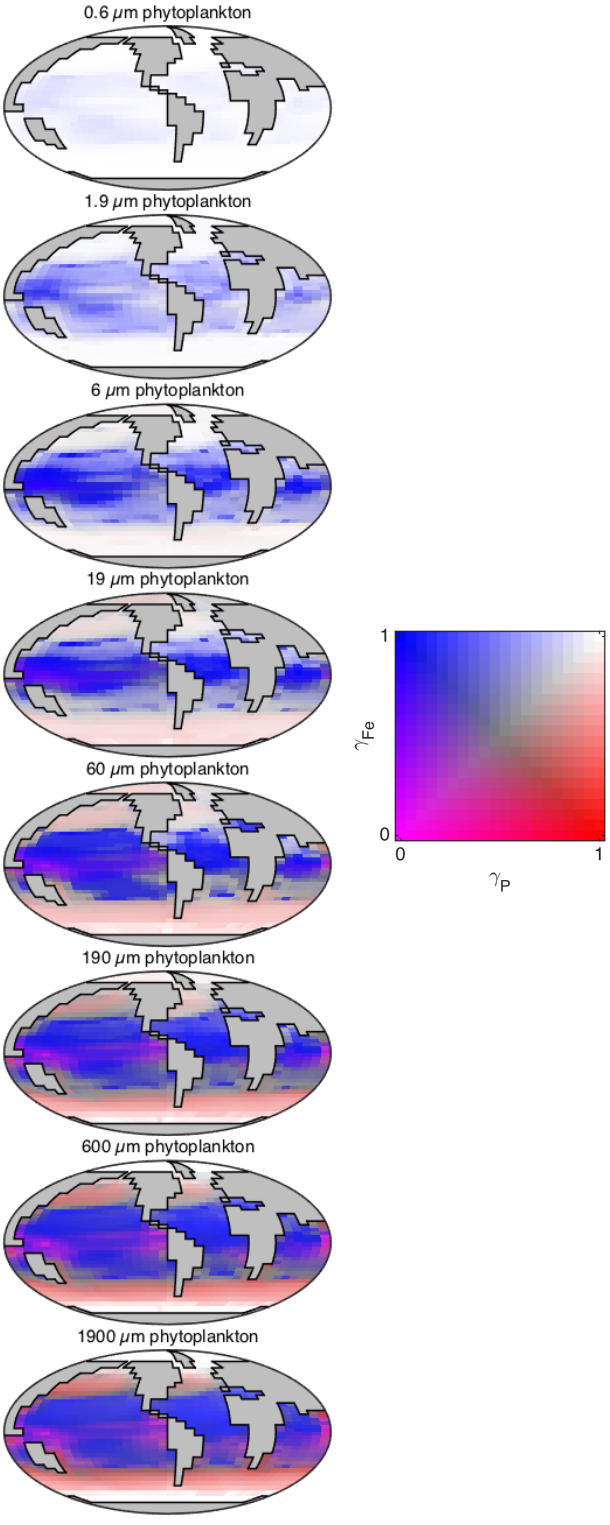

Figure 16. Nutrient limitation in each phytoplankton population. The two-dimensional colour-scale indicates decreasing phosphorus limitation from left to right, and decreasing iron limitation from bottom to top. White is therefore nutrient replete, blue is phosphorus limited, red is iron limited, and magenta is phosphorus-iron co-limited.

5.2.2 Time-series

The seasonal cycles of phytoplankton chlorophyll *a* are compared to time-series observations in Figure 18. The modelled total chlorophyll concentrations (black lines) track the observed concentrations (red dots) reasonably well at most sites, and perhaps better than might be expected from the comparison to satellite data in Figure 14. The modelled surface chlorophyll concentration is probably too low in the equatorial Pacific, while the spring bloom occurs one to two months earlier than was seen during the North Atlantic Bloom Experiment.

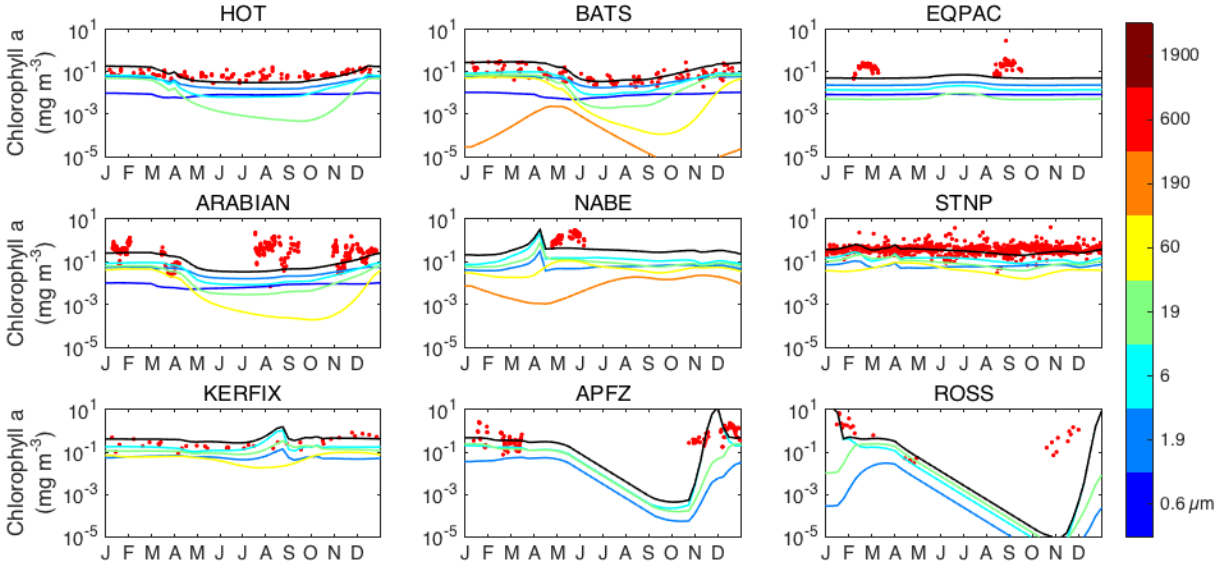

Figure 17. Annual cycle of surface chlorophyll *a* at nine JGOFS time-series sites. Red dots indicate climatological observations, while the black lines represents modelled total surface chlorophyll *a*. Coloured lines represent chlorophyll *a* in individual size classes (blue = small, red = large). Locations of the time-series are indicated in Figure 6.

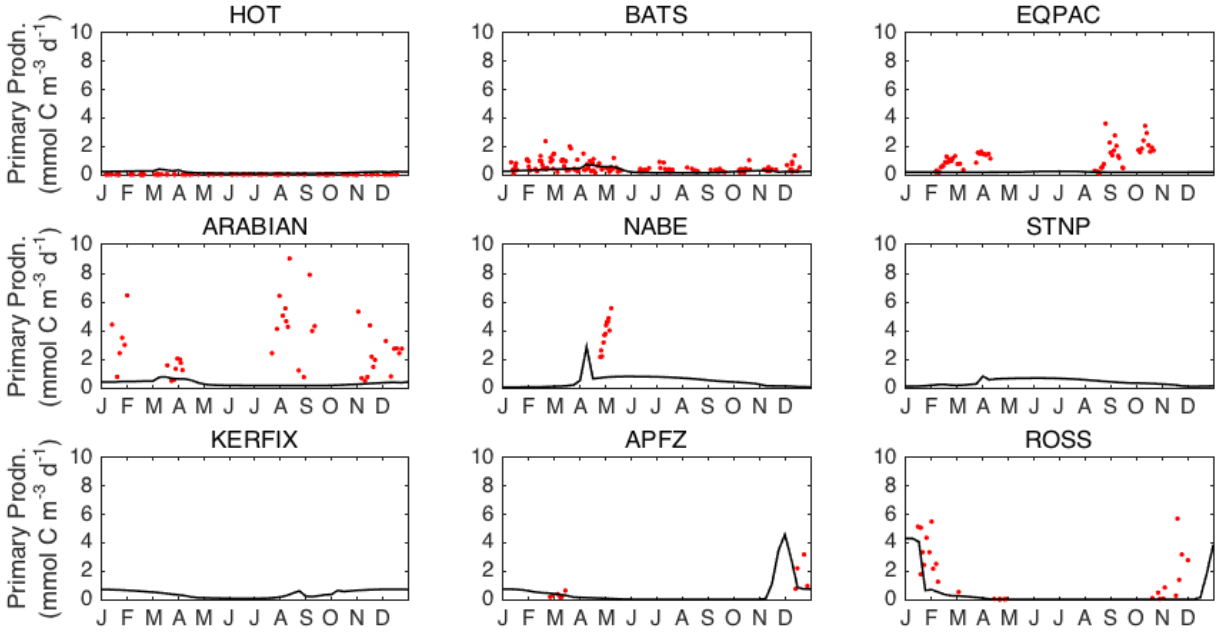

Figure 18. Annual cycle of surface primary production at nine JGOFS time-series sites. Red dots indicate climatological observations, while the black lines represents modelled total primary production. Locations of the time-series are indicated in Figure 6.

5.2.3 BIOGEM vs. ECOGEM

Figure 19 is a Taylor digram comparing the two models in terms of their correlation to observations and their standard deviations, relative to observations. A perfect model would be located at the middle of the bottom axis, with a correlation coefficient of 1.0 and a normalised standard deviation of 1.0. The closer a model is to this ideal point, the better a representation of the data it provides. Figure 19 shows that ECOGEM is located further from the ideal point than BIOGEM, in terms of oxygen, alkalinity, phosphate, and DIC. The new model seems to provide a universally worse representation of global ocean biogeochemistry. This is perhaps not surprising, given that BIOGEM has been systematically tuned to match the observation data in question (Ridgwell et al., 2007). ECOGEM has not yet been optimised in this way.

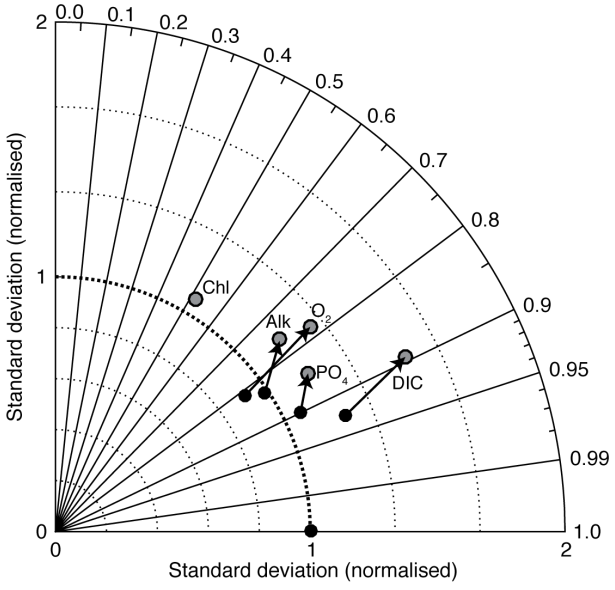

Figure 19. Taylor diagram comparing BIOGEM and ECOGEM to annual mean observation fields.

6 Discussion

The marine ecosystem is a central component of the Earth system, harnessing solar energy to sustain the biogeochemical cycling of elements between dissolved inorganic nutrients, living biomass and decaying organic matter. The interaction of these components with the global carbon cycle is critical to our interpretation of past, present and future climates, and has motivated the development of a wide range of models. These can be placed on a spectrum of increasing complexity, from simple and computationally efficient box models to fully coupled Earth system models with extremely large computational overheads.

GEnIE is a model of intermediate complexity on this spectrum. It has been designed to allow rapid model evaluation while at the same time retaining somewhat realistic global dynamics that facilitate comparison with observations. With this goal in mind, the biological pump was parameterised as a simple vertical flux defined as a function of environmental conditions (Ridgwell et al., 2007). This simplicity is well suited to questions concerning the interactions of marine biogeochemistry and climate, but at the same time precludes any investigation of the role of ecological interactions with the broader Earth system.

Here we have presented an ecological extension to GEnIE that opens up this area of investigation. The ecological model is rooted in size-dependent physiological and ecological constraints (Ward et al., 2012). The ecophysiological parameters are relatively well constrained by observations, even in comparison to simpler ecosystem models that are based on much more aggregated functional groups (Anderson, 2005; Litchman et al., 2007). The size-based formulation has the additional benefit of linking directly to functional aspects of the ecosystem, such as food-web structure and particle sinking (Ward and Follows, 2016).

The aim of this paper is to provide a detailed description of the new ecological component. It is clear from Figure 19 that the switch from the parameterised biological pump to the explicit ecological model has led to a deterioration in the overall ability of GEnIE to reproduce the global distributions of important biogeochemical tracers. This is an acceptable outcome, as our goal here is simply to provide a full description of the new model. Given that the original model was calibrated to the observations in question (Ridgwell et al., 2007), that process will need to be repeated for the new model before any sort of objective comparison can be made.

Despite the overall deterioration in terms of model-observation misfit, the biogeochemical components of the model retain the key features that should be expected. At the same time, the ecological community conforms to expectations in terms of standing stocks and fluxes, both in terms of large-scale spatial distributions, and the seasonal cycles at specific locations. Overall patterns of community structure and physiological limitation also follow expectations based on observations and theory.

As presented, the model is limited to three limiting resources (light, phosphorus, and iron) and two plankton functional types (phytoplankton and zooplankton). We have written the model equations

to facilitate the extension of the model to include additional components. In particular, the model capabilities can be extended by enabling silicon and nitrogen limitation, leveraging the silicon and nitrogen cycles already present in BIOGEM (Monteiro et al., 2012). Adding these nutrients will enable the addition of diatoms and diazotrophs, which are both likely to be important factors affecting the strength of the long-term biological pump (Tyrrell, 1999; Armstrong et al., 2002).

7 Code availability

The model code and user instructions can be found at http://www.seao2.info/mycgenie.html.

SVN number ????

Acknowledgements. This work was supported by the European Research Council 'PALEOGENiE' project (ERC-2013-CoG-617313). BAW thanks the Marine Systems Modelling group at the National Oceanography Centre, Southampton.

References

Anderson, T. R.: Plankton functional type modelling: Running before we can walk?, Journal of Plankton Research, 27, 1073–1081, 2005.

Anderson, T. R. and Pondaven, P.: Non-Redfield carbon and nitrogen cycling in the Sargasso Sea: pelagic imbalances and export flux, Deep-Sea Research I, 50, 573–591, 2003.

Armstrong, R. A., Lee, C., Hedges, J. I., Honjo, S., and Wakeham, S. G.: A new, mechanistic model for organic carbon fluxes in the ocean based on the quantitative association of POC with ballast materials, Deep-Sea Research II, 49, 219–236, 2002.

Aumont, O., Maier-Reimer, E., Blain, S., and Pondaven, P.: An ecosystem model of the global ocean including Fe, Si, P co-limitations, Global Biogeochemical Cycles, 17, doi:10.1029/2001GB001 745, 2003.

Baas-Becking, L. G. M.: Geobiologie of Inleiding Tot de Milieukunde, Van Stockum & Zoon, The Hague, 1934.

Bacastow, R. and Maier-Reimer, E.: Ocean-circulation model of the carbon cycle, Climate Dynamics, 4, 95–125, 1990.

Behrenfeld, M. J. and Falkowski, P. G.: Photosynthetic rates derived from satellite-based chlorophyll concentration, Limnology and Oceanography, 42, 1–20, 1997.

Billet, D. S. M., Lampitt, R. S., Rice, A. L., and Mantoura, R. F. C.: Seasonal sedimentation of phytoplankton to the deep sea benthos, Nature, 302, 1983.

Bruggeman, J. and Kooijman, S. A. L. M.: A biodiversity-inspired approach to aquatic ecosystem modeling, Limnology and Oceanography, 52, 1533–1544, 2007.

Cao, L., Eby, M., Ridgwell, A., Caldeira, K., Archer, D., Ishida, A., Joos, F., Matsumoto, K., Mikolajewicz, U., Mouchet, A., Orr, J. C., Plattner, G.-K., Schlitzer, R., Tokos, K., Totterdell, I., Tschumi, T., Yamanaka, Y., and Yool, A.: The role of ocean transport in the uptake of anthropogenic CO_2, Biogeosciences, 6, 375–390, doi:10.5194/bg-6-375-2009, http://www.biogeosciences.net/6/375/2009/, 2009.

Caperon, J.: Growth response of *Isochrysis galbana* to nitrate variation at limiting concentrations, Ecology, 49, 886–872, 1968.

Carr, M.-E., Friedrichs, M. A. M., Schmeltz, M., Aita, M. N., Antoine, D., Arrigo, K. R., Asanuma, I., Aumont, O., Barber, R., Behrenfeld, M., Bidigare, R., Buitenhuis, E. T., Campbell, J., Ciotti, A., Dierssen, H., Dowell, M., Dunne, J., Esaias, W., Gentili, B., Gregg, W., Groom, S., Hoepffner, N., Ishizaka, J., Kameda, T., le Quéré, C., Lohrenz, S., Marra, J., Mélin, F., Moore, K., Morel, A., Reddy, T. E., Ryan, J., Scardi, M., Smyth, T., Turpie, K., Tilstone, G., Waters, K., and Yamanaka, Y.: A comparison of global estimates of marine primary production from ocean color, Deep-Sea Research II, 53, 541–770, 2006.

Dierssen, H. M.: Perspectives on empirical approaches for ocean color remote sensing of chlorophyll in a changing climate, Proceedings of the National Academy of Sciences of the United States of America, 107, 17 073–17 078, 2010.

Droop, M. R.: Vitamin B12 and Marine Ecology, IV. The kinetics of uptake, growth and inhibition in *Monochrysis lutheri*, Journal of the Marine Biological Association of the United Kingdom, 48, 689–733, 1968.

Edwards, N. and Marsh, R.: Uncertainties due to transport-parameter sensitivity in an efficient 3-D ocean-climate model, Climate Dynamics, 24, 415–433, 2005.

Fasham, M. J. R., Ducklow, H. W., and McKelvie, S. M.: A nitrogen-based model of plankton dynamics in the oceanic mixed layer, Journal of Marine Research, 48, 591–639, 1990.

Flynn, K. J.: The importance of the form of the quota curve and control of non-limiting nutrient transport in phytoplankton models, Journal of Plankton Research, 30, 423–438, 2008.

Follows, M. J., Dutkiewicz, S., Grant, S., and Chisholm, S. W.: Emergent Biogeography of Microbial Communities in a Model Ocean, Science, 315, 1843–1846, 2007.

Friedrichs, M. A. M., Hood, R. R., and Wiggert, J. D.: Ecosystem model complexity versus physical forcing: Quantification of their relative impact with assimilated Arabian Sea data, Deep-Sea Research II, 53, 576–600, 2006.

Friedrichs, M. A. M., Dusenberry, J. A., Anderson, L. A., Armstrong, R., Chai, F., Christian, J. R., Doney, S. C., Dunne, J., Fujii, M., Hood, R. R., McGillicuddy, D., Moore, J. K., Schartau, M., Spitz, Y. H., and Wiggert, J. D.: Assessment of skill and portability in regional marine biogeochemical models: the role of multiple planktonic groups, Journal of Geophysical Research, 112, 2007.

Geider, R. J., MacIntyre, H. L., and Kana, T. M.: A dynamic regulatory model of phytoacclimation to light, nutrients and temperature, Limnology and Oceanography, 43, 679–694, 1998.

Gibbs, S. J., Bown, P. R., Ridgwell, A., Young, J. R., Poulton, A. J., and O'Dea, S. A.: Ocean warming, not acidification, controlled coccolithophore response during past greenhouse climate change., Geology, 44, 59 – 62, doi:10.1130/G37273.1, 2015.

Guidi, L., Stemmann, L., Jackson, G. A., Ibanez, F., Claustre, H., Legendre, L., Picheral, M., and Gorsky, G.: Effects of phytoplankton community on production, size and export of large aggregates: A world-ocean analysis, Limnology and Oceanography, 54, 1951–1963, 2009.

Hain, M. P., Sigman, D. M., and Haug, G. H.: The biological pump in the past, in: Treatise on Geochemistry, vol. 8, pp. 485–517, Elsevier, 2nd edn., 2014.

Hansen, P. J., Bjrnsen, P. K., and Hansen, B. W.: Zooplankton grazing and growth: Scaling with the 2-2,000-μm body size range, Limnology and Oceanography, 42, 678–704, 1997.

Hargreaves, J. C., Annan, J. D., Edwards, N. R., and Marsh, R.: An efficient climate forecasting method using an intermediate complexity Earth System Model and the ensemble Kalman filter, Climate Dynamics, 23, 745–760, doi:10.1007/s00382-004-0471-4, http://dx.doi.org/10.1007/s00382-004-0471-4, 2004.

Hollowed, A. B., Barange, M., Beamish, R. J., Brander, K., Cochrane, K., Drinkwater, K., Foreman, M. G. G., Hare, J. A., Holt, J., Ito, S., Kim, S., King, J., Loeng, H., MacKenzie, B. R., Mueter, F. J., Okey, T. A., Peck, M. A., Radchenko, V. I., Rice, J. C., Schirripa, M. J., Yatsu, A., and Yamanaka, Y.: Projected impacts of climate change on marine fish and fisheries, ICES Journal of Marine Science, 5, 1023–1037, 2013.

Hood, R. R., Laws, E. A., Armstrong, R. A., Bates, N. R., Brown, C. W., Carlson, C. A., Chai, F., Doney, S. C., Falkowski, P. G., Feely, R. A., Friedrichs, M. A. M., Landry, M. R., Moore, J. K., Nelson, D. M., Richardson, T. L., Salihoglu, B., Schartau, M., Toole, D. A., and Wiggert, J. D.: Pelagic functional group modelling: Progress, challenges and prospects, Deep-Sea Research II, 53, 459–512, 2006.

John, E., Wilson, J., Pearson, P., and Ridgwell, A.: Temperature-dependent remineralization and carbon cycling in the warm Eocene oceans, Palaeogeography, Palaeoclimatology, Palaeoecology, 413, 158 – 166, doi:http://dx.doi.org/10.1016/j.palaeo.2014.05.019, http://www.sciencedirect.com/science/article/pii/S0031018214002685, selected Papers, Geologic Problem Solving with Microfossils3, 2014.

Kraus, E. B. and Turner, J. S.: A one-dimensional model of the seasonal thermocline II. The general theory and its consequences, Tellus, 19, 98–106, 1967.

Kwiatkowski, L., Yool, A., Allen, J. I., Anderson, T. R., Barciela, R., Buitenhuis, E. T., Butenschön, M., Enright, C., Halloran, P. R., Quéré, C. L., de Mora, L., Racault, M.-F., Sinha, B., Totterdell, I. J., , and Cox, P. M.: iMarNet: an ocean biogeochemistry model intercomparison project within a common physical ocean modelling framework, Biogeosciences, 11, 7291–7304, 2014.

Le Quéré, C., Harrison, S. P., Prentice, I. C., Buitenhuis, E. T., Aumont, O., Bopp, L., Claustre, H., Cotrim da Cunha, L., Geider, R., Giraud, X., Klaas, C., Kohfeld, K. E., Legendre, L., Manizza, M., Platt, T., Rivkin, R. B., Sathyendranath, S., Uitz, J., Watson, A. J., and Wolf-Gladrow, D.: Ecosystem dynamics based on plankton functional types for global ocean biogeochemistry models, Global Change Biology, 11, 2016–2040, 2005.

Litchman, E., Klausmeier, C. A., Schofield, O. M., and Falkowski, P. G.: The role of functional traits and trade-offs in structuring phytoplankton communities: scalling from cellular to ecosystem level, Ecology Letters, 10, 1170–1181, 2007.

Maier-Reimer, E.: Geochemical cycles in an ocean general circulation model. Preindustrial tracer distributions, Global Biogeochemical Cycles, 7, 645–677, 1993.

Marsh, R., Müller, S. A., Yool, A., and Edwards, N. R.: Incorporation of the C-GOLDSTEIN efficient climate model into the GENIE framework: "eb_go_gs" configurations of GENIE, Geoscientific Model Development, 4, 957–992, doi:10.5194/gmd-4-957-2011, http://www.geosci-model-dev.net/4/957/2011/, 2011.

Martin, J. H., Knauer, G. A., Karl, D. M., and Broenkow, W. W.: Vertex: carbon cycling in the northeast Pacific, Deep-Sea Research, 34, 267–285, 1987.

Meyer, K. M., Ridgwell, A., and Payne, J. L.: The influence of the biological pump on ocean chemistry: implications for long-term trends in marine redox chemistry, the global carbon cycle, and marine animal ecosystems, Geobiology, 14, 207–219, doi:10.1111/gbi.12176, http://dx.doi.org/10.1111/gbi.12176, 2016.

Monteiro, F. M., Follows, M. J., and Dutkiewicz, S.: Distribution of diverse nitrogen fixers in the global ocean., Global Biogeochemical Cycles, 24, doi:10.1029/2009GB003 731, 2010.

Monteiro, F. M., Pancost, R. D., Ridgwell, A., and Donnadieu, Y.: Nutrients as the dominant control on the spread of anoxia and euxinia across the Cenomanian-Turonian oceanic anoxic event (OAE2): Model-data comparison, Paleoceanography, 27, n/a–n/a, doi:10.1029/2012PA002351, http://dx.doi.org/10.1029/2012PA002351, pA4209, 2012.

Monteiro, F. M., Bach, L. T., Brownlee, C., Bown, P., Rickaby, R. E. M., Tyrrell, T., Beaufort, L., Dutkiewicz, S., Gibbs, S., Gutowska, M. A., Lee, R., Poulton, A. J., Riebesell, U., Young, J., and Ridgwell, A.: Calcification in marine phytoplankton: Physiological costs and ecological benefits, Science Advances, 2016.

Moore, C. M., Mills, M. M., Arrigo, K. R., Berman-Frank, I., Bopp, L., Boyd, P. W., Galbraith, E. D., Geider, R. J., Guieu, C., Jaccard, S. L., Jickells, T. D., Roche, J. L., Lenton, T. M., Mahowald, N. M., Marañón, E., Marinov, I., Moore, J. K., Nakatsuka, T., Oschlies, A., Saito, M. A., Thingstad, T. F., Tsuda, A., and Ulloa, O.: Processes and patterns of oceanic nutrient limitation, Nature Geoscience, 2013.

Moore, J. K., Doney, S. C., Kleypas, J. A., Glover, D. M., and Fung, I. Y.: An intermediate complexity marine ecosystem model for the global domain, Deep-Sea Research II, 49, 403–462, 2002.

Najjar, R. G., Sarmiento, J. L., and Toggweiler, J. R.: Downward transport and fate of organic matter in the ocean: Simulations with a general circulation model, Global Biogeochemical Cycles, 6, 45–76, 1992.

Norris, R., Kirtland Turner, S., Hull, P., and Ridgwell, A.: Marine ecosystem responses to Cenozoic global change., Science, 341, doi:DOI: 10.1126/science.1240543, 2013.

Oschlies, A.: Model-derived estimates of new production: New results point to lower values, Deep-Sea Research II, 48, 2173–2197, 2001.

Oschlies, A.: Ocean Weather Forecasting, chap. On the use of data assimilation in biogeochemical modelling, pp. 525–557, Springer, 2006.

Padisák, J., Soróczki-Pintér, E., and Rezner, Z.: Sinking properties of phytoplankton shapes and the relation of form resistance to morphological diversity of plankton - An experimental study, Hydrobiologia, 500, 243–257, 2003.

Palmer, J. R. and Totterdell, I. J.: Production and export in a global ocean ecosystem model, Deep-Sea Research I, 48, 1169–1198, 2001.

Parekh, P., Follows, M. J., Dutkiewicz, S., and Ito, T.: Physical and biological regulation of the soft tissue carbon pump, Paleoceanography, 21, doi:10.1029/2005PA001 258, 2006.

Ridgwell, A. and Death, R.: Iron limitation in an efficient model of global carbon cycling and climate, in prep.

Ridgwell, A. and Schmidt, D. N.: Past constraints on the vulnerability of marine calcifiers to massive carbon dioxide release, Nature Geoscience, 3, 196–200, http://dx.doi.org/10.1038/ngeo755, 2010.

Ridgwell, A., Hargreaves, J. C., Edwards, N. R., Annan, J. D., Lenton, T. M., Marsh, R., Yool, A., and Watson, A.: Marine geochemical data assimilation in an efficient Earth System Model of global biogeochemical cycling, Biogeosciences, 4, 87–104, doi:10.5194/bg-4-87-2007, http://www.biogeosciences.net/4/87/2007/, 2007.

Schartau, M. and Oschlies, A.: Simultaneous data-based optimization of a 1D-ecosystem model at three locations in the North Atlantic: Part II - Standing stocks and nitrogen fluxes, Journal of Marine Research, 61, 795–821, 2003.

Smayda, T. J.: The suspension and sinking of phytoplankton in the sea, Oceanography and Marine Biology: An Annual Review, 8, 1970.

Spitz, Y. H., Moisan, J. R., and Abbot, M. R.: Configuring an ecosystem model using data from the Bermuda Atlantic Time Series (BATS), Deep-Sea Research II, 48, 1733–1768, 2001.

Tagliabue, A., Mtshali, T., Aumont, O., Bowie, A. R., Klunder, M. B., Roychoudhury, A. N., and Swart, S.: A global compilation of dissolved iron measurements: focus on distributions and processes in the Southern Ocean, Biogeosciences, 9, 233–2349, 2012.

Tagliabue, A., Aumont, O., DeAth, R., Dunne, J. P., Dutkiewicz, S., Galbraith, E., Misumi, K., Moore, J. K., Ridgwell, A., Sherman, E., Stock, C., Vichi, M., Völker, C., and Yool, A.: How well do global ocean biogeochemistry models simulate dissolved iron distributions?, Global Biogeochemical Cycles, 30, 149–174, doi:10.1002/2015GB005289, http://dx.doi.org/10.1002/2015GB005289, 2015GB005289, 2016.

Tang, E. P. Y.: The allometry of algal growth rates, Journal of Plankton Research, 17, 1325–1335, 1995.

Tyrrell, T.: The relative influences of nitrogen and phosphorous on oceanic primary production, Nature, 400, 525–531, 1999.

Ward, B. A. and Follows, M. J.: Marine mixotrophy increases trophic transfer efficiency, net community production and carbon export, Proceedings of the National Academy of Sciences of the United States of America, 113, 2958–2963, 2016.

Ward, B. A., Friedrichs, M. A. M., Anderson, T. R., and Oschlies, A.: Parameter optimisation and the problem of underdetermination in marine biogeochemical models, Journal of Marine Systems, 81, 34–43, 2010.

Ward, B. A., Dutkiewicz, S., Jahn, O., and Follows, M. J.: A size structured food-web model for the global ocean, Limnology and Oceanography, 57, 1877–1891, 2012.

Westberry, T., Behrenfeld, M. J., Siegel, D. A., and Boss, E.: Carbon-based primary productivity modeling with vertically resolved photoacclimation, Global Biogeochemical Cycles, 22, GB2024, 2008.

Wroblewski, J. S., Sarmiento, J. L., and Flierl, G. R.: An ocean basin scale model of plankton dynamics in the North Atlantic. 1. Solutions for the climatological oceanographic conditions in May, Global Biogeochemical Cycles, 2, 199–218, 1988.

Yool, A., Popova, E. E., and Anderson, T. R.: MEDUSA-2.0: an intermediate complexity biogeochemical model of the marine carbon cycle for climate change and ocean acidification studies, Geoscientific Model Development, 6, 1767–1811, 2013.